

RESEARCH ARTICLE

10.1002/2015JB012355

Key Points:

- The 1739 Yinchuan earthquake occurred on the East Helanshan Fault
- The earthquake had a magnitude in the range 7.1 to 7.6
- Valuable to combine historical earthquake accounts with geological observations

Correspondence to:

T. A. Middleton,
tim.middleton@earth.ox.ac.uk

Citation:

Middleton, T. A., R. T. Walker, B. Parsons, Q. Lei, Y. Zhou, and Z. Ren (2016), A major, intraplate, normal-faulting earthquake: The 1739 Yinchuan event in northern China, *J. Geophys. Res. Solid Earth*, 121, 293–320, doi:10.1002/2015JB012355.

Received 14 JUL 2015

Accepted 7 DEC 2015

Accepted article online 14 DEC 2015

Published online 5 JAN 2016

A major, intraplate, normal-faulting earthquake: The 1739 Yinchuan event in northern China

Timothy A. Middleton¹, Richard T. Walker¹, Barry Parsons¹, Qiyun Lei², Yu Zhou¹, and Zhikun Ren³
¹COMET, Department of Earth Sciences, University of Oxford, Oxford, UK, ²Ningxia Seismological Bureau, Yinchuan, China,

³State Key Laboratory of Earthquake Dynamics, Institute of Geology, China Earthquake Administration, Beijing, China

Abstract A large continental normal-faulting earthquake occurred in the Yinchuan Graben in northern China on 3 January 1739. This event is of significant interest for two reasons. First, it has been suggested on the basis of historical records of shaking that this was a magnitude 8.0 event. If this is true, the 1739 earthquake would be one of the largest continental normal-faulting earthquakes ever recorded, and this should prompt us to consider the factors contributing to its unusual size. Second, there has been some debate in the literature about the causative structure, with at least three different faults posited as the seismogenic source. We use five ¹⁴C ages to date a series of scarps on the East Helanshan Fault, which lies to the west of the graben, and bracket the scarp formation to the last 350 years. We use high-resolution, stereo imagery from the Pleiades satellites to build a 1 to 2 m resolution DEM of the fault and combine this with field observations to map the East Helanshan rupture in detail. We then construct a throw distribution, determine the slip vector azimuth, and reassess the earthquake magnitude using simple scaling relationships. We conclude that the 1739 earthquake occurred on the East Helanshan Fault, had a rupture length of approximately 87 km, a maximum throw of 5.1 m, and an average throw of 3.0 m, yielding a best estimate magnitude in the range M_w 7.1 to M_w 7.6. We suggest that the previous magnitude estimates are biased by enhanced shaking of the sediments within the Yinchuan Graben.

1. Introduction

Continental normal-faulting earthquakes greater than magnitude 7.0 are uncommon. The few recent examples include: the M 7.6 1915 Pleasant Valley (Nevada) event [Jackson and Leeder, 1994], the M 7.9 1957 Muya (Siberia) event [Molnar and Deng, 1984], the M 7.3 1959 Hebgen Lake (Montana) event [Jackson and White, 1989], and the M 7.0 2006 Mozambique event [Copley et al., 2012]. Studying large normal-faulting earthquakes is challenging: they typically occur in slowly deforming regions with long repeat times, and very few of them have occurred during the instrumental period. Nonetheless, though these events are comparatively infrequent, their large sizes mean that they pose a significant seismic hazard, particularly in densely populated areas. In order to expand the catalogue of such events, we need to look further back into history. However, historical records alone are not sufficient to allow us to estimate reliable fault parameters and earthquake magnitudes. It is therefore important that the interpretation of historical records is combined with geological observations made in the field.

In this paper we focus on the 1739 Yinchuan earthquake, located on the western side of the Ordos Plateau in northern China (see Figure 1), in which 50,000 people are thought to have been killed [Zhang et al., 1986]. The recorded intensities of shaking (see Figures 1 and 2) have previously been combined with empirical relationships to suggest that this was a magnitude 8.0 event [Zhang et al., 1986; State Seismological Bureau and Fudan University, 1990] and many subsequent authors have since assumed that this is the correct magnitude [e.g., Deng and Liao, 1996; Bai and Jiao, 2005; Lin et al., 2013; Lei et al., 2015 and Lin et al., 2015]. If the magnitude of the Yinchuan earthquake has been correctly estimated it would be among the largest continental normal-faulting earthquakes ever recorded. The city of Yinchuan now has a population of nearly 2 million people and a similarly large event in future is likely to be even more destructive.

M_w 8.0 equates to a seismic moment of 1.11×10^{21} Nm. Previous studies have indicated a rupture length of around 88 km [Deng and Liao, 1996] and, using the relationship $M_0 = \mu A \bar{u}$ (where μ is the modulus of rigidity, A is the fault plane area, and \bar{u} is the average slip [Hanks and Kanamori, 1979]), this would suggest fault slip of 10 to 13 m and a slip-to-length ratio of between 1.1 and 1.5×10^{-4} (using a fault dip of 39° and different

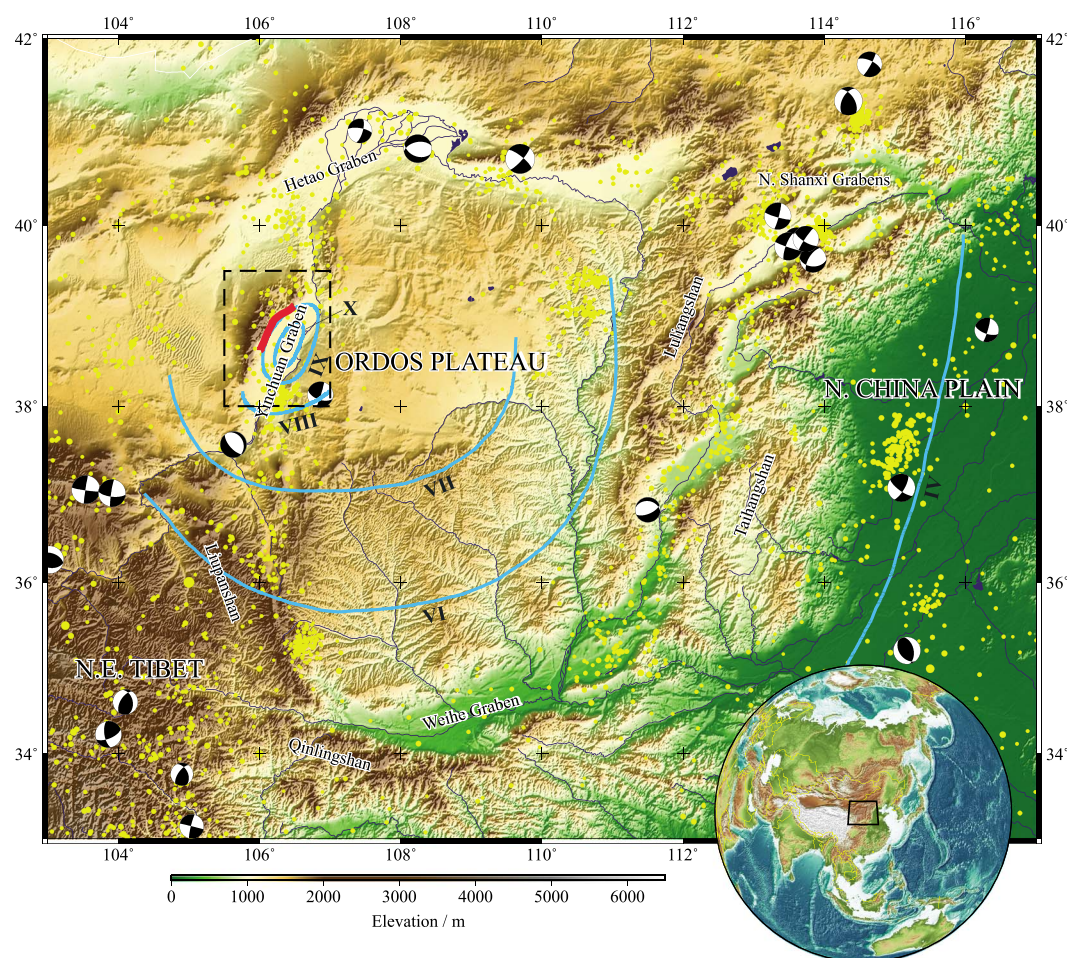


Figure 1. SRTM topography [Farr and Kobrick, 2000] of the Ordos Plateau in northeastern China. Focal mechanisms from the Global CMT catalogue [Ekström *et al.*, 2012] are shown for recent earthquakes with magnitudes greater than M_w 5.0. Earthquakes of M_w 2.0–5.0 from the ISC catalogue [International Seismological Centre, 2013] are shown as yellow dots. Rivers are indicated in dark blue, and inset globe shows the location of Figure 1 within Asia. The East Helanshan Fault is highlighted in red and isoseismals for the 1739 earthquake according to the new Chinese intensity scale are shown in light blue [State Seismological Bureau and Fudan University, 1990]. The dotted black box indicates the region shown in Figure 2.

seismogenic thicknesses of 20 and 28 km, respectively). These values are somewhat larger than typical slip-to-length ratios which are of the order of 10^{-5} to 10^{-4} [Scholz, 1982, 2002]. Unusually large slip-to-length ratios have been seen elsewhere— 2.2×10^{-4} for the Assam earthquake [Bilham and England, 2001], and around 3×10^{-4} for the Bhuj earthquake [Copley *et al.*, 2011]—but such examples are rare. If the Yinchuan earthquake is really as large as cited and does have such a large slip-to-length ratio, then the factors that contributed to such an unusual event deserve detailed consideration. Additionally, there has been some disagreement in the literature about the causative fault for the 1739 earthquake; the East Helanshan, Yinchuan-Pingluo, and Yellow River Faults have all been suggested (see section 3) [Zhang *et al.*, 1986; Deng and Liao, 1996; Bai and Jiao, 2005; Chai *et al.*, 2006; Lin *et al.*, 2013; Lei *et al.*, 2015; Lin *et al.*, 2015].

Here prompted by recent debate on the causative fault, we examine the source parameters of the 1739 earthquake and use ^{14}C dating of Holocene material to provide further support for the East Helanshan Fault being the causative fault (see Figure 2). We use high-resolution (0.5 m) stereo imagery from the Pleiades satellites to produce a 1 to 2 m resolution digital elevation model (DEM) of the entire length of the East Helanshan Fault (see section 4 for a discussion of the resolution of the DEM) and combine this with new field observations to map the scarps along the range front in detail. The high-resolution topography enables us to identify and

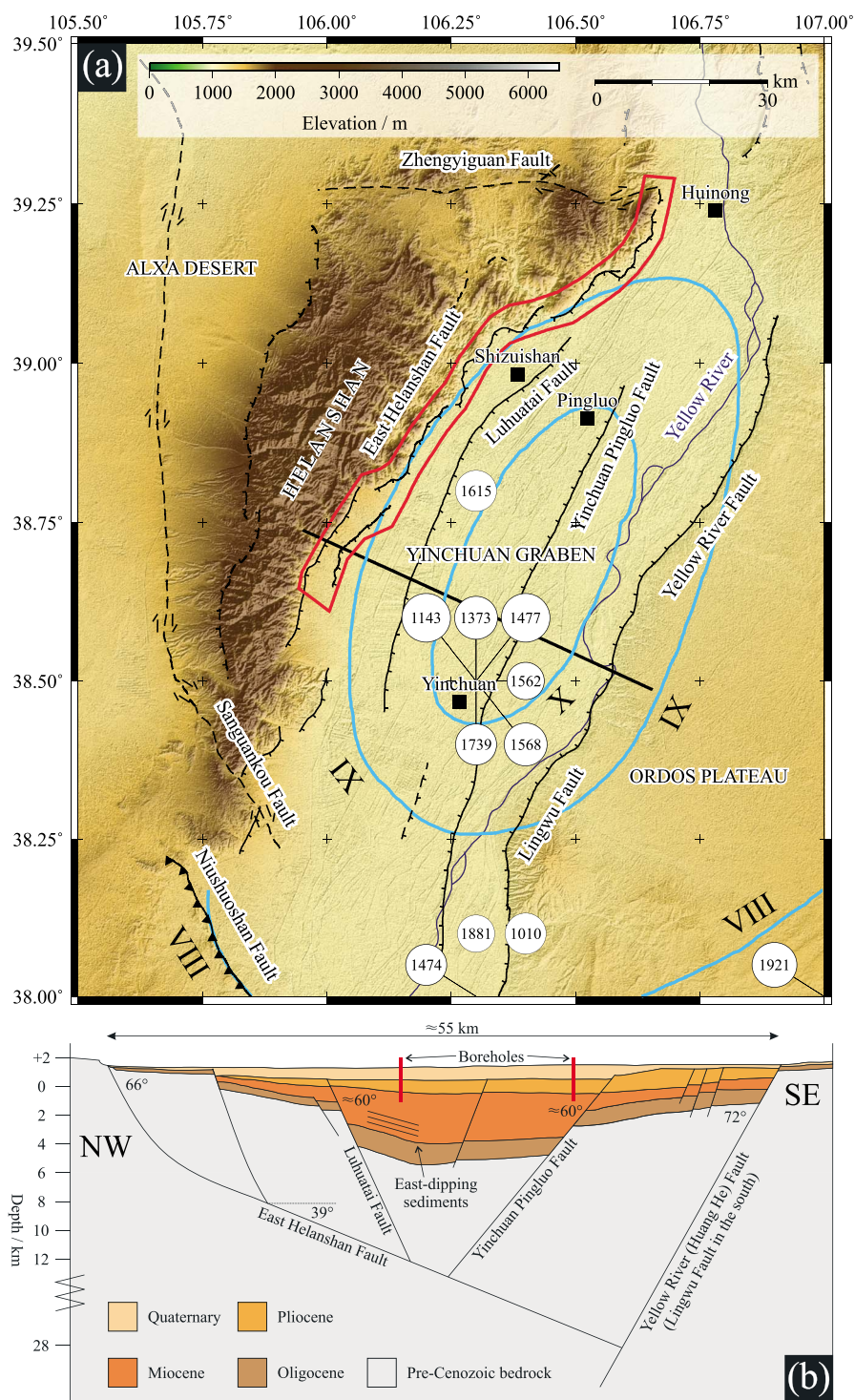


Figure 2. (a) ASTER GDEM topography of the Yinchuan Graben. Faults, marked as thin black lines, have been mapped from satellite imagery (source: <http://earth.google.com>) based upon earlier fault maps from *Tapponnier and Molnar* [1977], *Zhang et al.* [1986] and *Deng and Liao* [1996]. Faults that are inferred or show no evidence of Quaternary activity are marked by dotted lines. Cities are marked by black squares. Historical earthquakes from *Lee et al.* [1976] and *Lee et al.* [1978] are shown by white circles, including the year in which they occurred. The Yellow River, which flows to the north, is marked in dark blue. Red outline indicates coverage of Pleiades data. Thick black line shows approximate location of profile in Figure 2b. Isoseismals for the 1739 earthquake according to the *new Chinese intensity scale* are shown in light blue [State Seismological Bureau and Fudan University, 1990]. (b) Sketch (interpretive) cross section across the Yinchuan Graben based on seismic reflection data and previous figures in *Liu et al.* [2008], *Fang et al.* [2009], *Lei et al.* [2014] and *Lei et al.* [2015]. Note that the depth scale is not linear.

make measurements of the scarps along this fault in many more locations than was previously possible from isolated field observations alone. Finally, we use our observations and measurements to construct a throw distribution, estimate the slip vector azimuth and reassess the magnitude of the event.

2. Tectonic Setting

2.1. Active Faulting

The Yinchuan Graben is approximately 50 km wide and 160 km long and lies at the northern end of Ningxia Province on the western side of the Ordos Plateau in northern China (see Figure 1). The graben is bounded by north-south trending normal faults (see Figure 2). On the western side of the graben lies the East Helanshan Fault, while the eastern side of the graben is bordered by the Yellow River (Huang He) Fault [Zhang *et al.*, 1986]. Few surface outcrops of the Yellow River Fault have been conclusively identified, though linear features are visible in satellite imagery and the structure has been confirmed on seismic reflection profiles [Liu *et al.*, 2008; Fang *et al.*, 2009; Lin *et al.*, 2015]. Further, parallel, normal faults exist within the graben itself, the most prominent of which are the Luhatai and Yinchuan-Pingluo Faults [Zhang *et al.*, 1986]. These structures are buried beneath Quaternary sediments but are inferred from the seismic reflection profiles across the graben [Liu *et al.*, 2008; Fang *et al.*, 2009].

The graben is bounded at its southern end by a series of strike-slip and reverse faults, including the Sanguankou and Niushoushan Faults, which strike northwest-southeast (see Figure 2a). These faults straddle the complex transition from compression in the northeastern corner of the Tibetan Plateau to apparently east-west extension in the Yinchuan Graben itself, as implied by the north-south normal faulting [Zhang *et al.*, 1990]. Meanwhile, to the north of the graben, the east-west Zhengyiguan right-lateral strike-slip fault cuts basement rocks in the Helanshan (Helan mountains) and potentially provides a structural termination at this end of the graben [Zhang *et al.*, 1986].

The Yinchuan Graben is thought to have extended at 2.9 ± 1.0 mm/a since the Pliocene, based on a cross-sectional area balance [Zhang *et al.*, 1998]. Unfortunately, the GPS data from Wang *et al.* [2001] and Li *et al.* [2003] is not sufficiently dense to provide reliable geodetic constraints on the rate of extension. The graben contains 1 to 1.6 km of Quaternary sediments and approximately 6 km of pre-Quaternary deposits that have accumulated since the late Eocene [Zhang *et al.*, 1990]. Zhao *et al.* [2007b] calculate sedimentation rates of approximately 0.1 mm/a from the Eocene to the Miocene, about 0.5 mm/a in the Pliocene, and around 0.6 mm/a in the Quaternary. However, comparing the extension rate measured by Zhang *et al.* [1998] to the sedimentation rate since the Pliocene suggests that either the basin is under-filled, or that the extension rate is an overestimate.

As well as the 1739 event, various other historical earthquakes have been documented in the Yinchuan Graben (see Figure 2) [Lee *et al.*, 1976, 1978; Liu *et al.*, 2011]. In particular, two events, with inferred magnitudes of approximately 6.5, occurred in 1143 and 1477. Many of these earthquakes plot on top of the city of Yinchuan, though this is presumably because they were only reported in the major population center at the time (see Figure 2a).

2.2. The Deep Structure of the Yinchuan Graben

Although work on the structure of the Yinchuan Graben extends back as far as the 1950s [Fang *et al.*, 2009], most of it was conducted by the petroleum industry and little has been reported in the academic literature. However, the deep structure of the Yinchuan Graben is of significant importance for this study because the dip and depth extent of the major faults place important constraints on the maximum magnitude of the earthquakes they can generate.

Liu *et al.* [2008] published a seismic reflection profile that extends to a depth of 5 s two-way travel time (TWTT), which roughly corresponds to a depth of 10 km. They show the East Helanshan, Luhatai, Yinchuan-Pingluo, and Yellow River Faults, and a few other minor faults. The faults appear to have steep dips (of approximately 60°) and do not extend below 5 s TWTT. The sediments on this profile appear to dip to the east, and they are thickest in the center of the basin, between the Luhatai and Yinchuan-Pingluo Faults (see Figure 2b). On the basis of this, and other unpublished profiles, a number of authors have drawn similar interpretive cross sections [e.g., Zhang *et al.*, 1986; He *et al.*, 2005; Zhao *et al.*, 2007a; Lei *et al.*, 2014 and Lei *et al.*, 2015].

The only deeper information comes from a second seismic reflection profile, which extends down to 15 s TWTT (approximately 50 km), published by Fang *et al.* [2009]. According to their interpretation, the East Helanshan

Fault dips at around 39° to the southeast and extends to a depth of 28 km, where it meets the Yellow River Fault, which dips at around 72° to the northwest (see Figure 2b). The Luhutai and Yinchuan-Pingluo Faults both retain relatively steep dips (approximately 60°) and intersect the East Helanshan Fault at depths of 12 and 18 km respectively. Fang *et al.* [2009] conclude that the Yellow River Fault is the major, graben-controlling structure, which would be consistent with the apparently east-dipping sediments shown by Liu *et al.* [2008] and the fact that the Yellow River is on the eastern side of the Yinchuan Graben (see Figure 2a). Nonetheless, given the relative lack of published seismic reflection data, our interpretive cross section in Figure 2b remains provisional, and we do not have tight constraints on the uncertainties associated with the internal graben structure.

The Helanshan reach a maximum elevation of 3557 m [Zhang *et al.*, 1990], but different suggestions have been made about the origin of this topography. Liu *et al.* [2010] used apatite fission track dating to determine that rapid uplift of the Helanshan began 10 to 12 Ma ago. This uplift was quickest in the north and immediately adjacent to the East Helanshan Fault, resulting in a tilting of the range toward the southwest. Some authors have therefore concluded that the entire topography of the Helanshan is due to footwall uplift on the East Helanshan Fault [e.g., He *et al.*, 2005]. However, the rocks exposed in the Helanshan are a remnant of the Western Ordos fold-and-thrust belt, which formed between the Early-Middle and Late Jurassic [Liu, 2000; Darby and Ritts, 2002]. It is therefore likely that at least some of the Helanshan topography predates extension in the Yinchuan Graben. The thin basin fill in the hanging wall of the East Helanshan Fault and its apparently shallow dip (as proposed by Fang *et al.* [2009]—see also Figure 2b) may be related to it reactivating one of a series of older reverse faults.

3. Background to the 1739 Earthquake

The Yinchuan earthquake took place on the 3 January 1739 at around 18:00 UTC [Zhang *et al.*, 1986]. Ground shaking in the center of the Yinchuan Graben, particularly around the cities of Yinchuan and Pingluo, reached intensity X on the *new Chinese intensity scale* (see Figures 1 and 2) and lasted for up to 2 h after the earthquake—presumably because of aftershocks [Zhang *et al.*, 1986; State Seismological Bureau and Fudan University, 1990]. Further aftershocks were recorded for a number of years after the earthquake, including a magnitude 5.5 event on 13 February 1739 [Zhang *et al.*, 1986]. In Yinchuan city the west and north pagodas were severely damaged, while in Pingluo the high temple was completely destroyed. In the zone of greatest shaking, which stretches between Yinchuan and Pingluo, historical documents also record: temples, pagodas, offices, houses, and city walls that all collapsed; surface cracks up to 100 m long; and some buildings which subsided by up to 7 m due to the shaking [Zhang *et al.*, 1986].

Given the number of faults in the Yinchuan Graben, the causative fault for the 1739 earthquake has been the subject of some debate in the literature. Some authors have attributed it to the Yinchuan-Pingluo Fault [Liao and Pan, 1982; Chai *et al.*, 2006; Lin *et al.*, 2013]. Their principal reason for doing so is that the surface projection of this buried fault runs north-northeast—south-southwest directly under the city of Yinchuan and appears to coincide with the zone of maximum shaking on the isoseismal map. However, the Yinchuan Graben is filled with over 7 km of sediments [Zhang *et al.*, 1990]. These sediments may have amplified the seismic waves during the earthquake, leading to greatest ground motion in the center of the graben regardless of the location of the causative fault. The isoseismals are also elongate in a direction that is parallel to all four faults in the graben, so their shape does not help to determine the fault responsible.

Others, meanwhile, believe that the Yellow River Fault was the causative fault [Li and Wan, 1984; Lin *et al.*, 2015]. Lin *et al.* [2015], for example, identified an 8 km stretch of the fault between 39.010°N , 106.884°E and 39.073°N , 106.906°E . They did not observe any fresh scarps, but they found an offset sand layer with a ^{14}C age of 2650 ± 30 years before present.

In 1965, though, a series of fresh earthquake scarps were discovered along the East Helanshan Fault, on the western side of the Yinchuan Graben, by the Northwest Seismic Expedition of the Chinese Academy of Sciences [Liao and Pan, 1982]. Deng and Liao [1996] subsequently identified four locations along the range front, at Suyukou, Xiashigou, Jianquan, and Hongguozigou, where scarps could be seen (see Figure 3). Numerous authors have therefore attributed the 1739 event to the East Helanshan Fault [Zhang *et al.*, 1982; Deng *et al.*, 1984; Zhang *et al.*, 1986; Deng and Liao, 1996; Bai and Jiao, 2005; Lei *et al.*, 2015]. Although it seems most likely that these fresh-looking scarps are the ones that relate to the 1739 event, this has not yet been corroborated by dating offset Holocene surfaces.

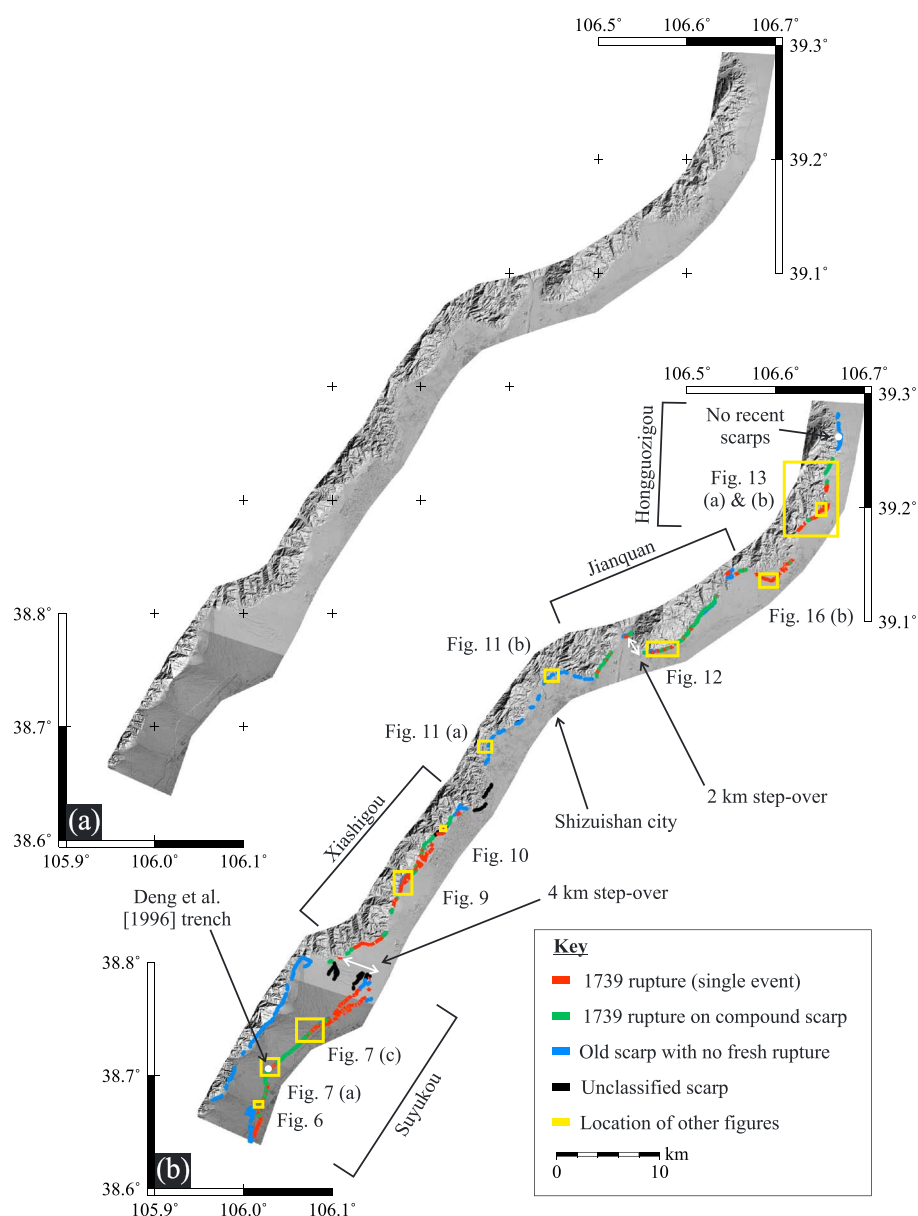


Figure 3. (a) High-resolution (1 to 2 m), shaded digital elevation model (DEM) of the East Helanshan Fault derived from Pleiades stereo imagery (location shown in Figure 2). (b) Annotated version of Figure 3a including mapped scarps and the locations of other figures.

A number of morphological observations of the scarps along the East Helanshan Fault have previously been made, largely on the Suyukou and Hongguozigou segments. *Deng and Liao* [1996] noted that the Xianshigou and Jianquan scarps offset the latest alluvial fans by 1 to 2 m, but little else is currently known about the scarps in these two locations.

The Suyukou scarps total around 16.5 km in length and lie 3 to 4 km southeast of the Helanshan range front, 30 km northwest of the city of Yinchuan [Deng and Liao, 1996]. The scarps vary in height up to a maximum of approximately 11 m, and the different levels have been interpreted to represent a series of normal-faulting earthquake ruptures within the Quaternary [Deng and Liao, 1996]. In this paper, however, we are only concerned with the lowest of these scarps, which is the one that may relate to the 1739 event. *Zhang et al.* [1986] and *Deng and Liao* [1996] obtained maximum single-event scarp heights at Suyukou of 4.6 m and 4.4 m, respectively. *Deng and Liao* [1996] also opened a number of trenches across the Suyukou scarps. They report results from one of these trenches (at 38.706°N, 106.028°E) in which they identify several colluvial wedges,

Table 1. Radiocarbon Dating Results^a

Sample Number	Location	Latitude (deg)	Longitude (deg)	Elevation (m)	Description	Age (¹⁴ C years BP)	Calibrated Date Range (years)
1	Road-cut site	106.01570	38.67350	1180	Faecal pellet	1.170 ± 0.004	Modern
2	Road-cut site	106.01570	38.67350	1180	Faecal pellet	1.158 ± 0.004	Modern
3	First river site	106.03300	38.71070	1227	Gymnosperm wood	279 ± 28	1514–1795 AD (95.4%)
4	First river site	106.03290	38.71080	1225	Charcoal	1130 ± 31	777–989 AD (95.4%)
5	Second river site	106.07449	38.74066	1187	Bivalve shell	2099 ± 31	199–45 BC (95.4%)

^aAll ¹⁴C samples were dated at the Oxford Radiocarbon Accelerator Unit (ORAU) at the Research Laboratory for Archaeology and the History of Art (RLAHA). Details of the methods used during sample preparation can be found in *Bronk et al.* [2004] and *Brock et al.* [2010].

the most recent of which they interpret to be from the 1739 event (see Figure 3 for location). They do not have age control on this most recent faulting event, but they have a ¹⁴C age for the previous colluvial wedge of 2720 ± 60 years before present. In addition, *Deng and Liao* [1996] measured surface fault dips in their trenches of between 65 and 85°, with an average of 75°.

The Hongguozigou scarps are 3.5 to 4 km long and lie some 65 km north of Suyukou along the Helanshan range front, about 12 km southwest of Huinong city [*Zhang et al.*, 1986; *Deng and Liao*, 1996]. *Zhang et al.* [1986] record a maximum single-event scarp height on this section of 5.3 m, with a typical average of 2 to 3 m. At the northern end of these scarps, three parallel fault strands intersect part of the Great Wall of China that dates from 1531, during the Ming Dynasty [*Ding*, 1981]. This site has been the cause of much controversy. Some authors argue that the Great Wall at this location was offset during the 1739 earthquake [e.g., *Zhang et al.*, 1986; *Deng and Liao*, 1996; *Lei et al.*, 2015], while other studies propose that it was built on top of preexisting scarps that were not reactivated in 1739 [e.g., *Lin et al.*, 2013, 2015]. The situation has been further confused by rebuilding of the wall and human landscape modification that has obscured much of the original field data.

4. Methods

4.1. ¹⁴C Dating

We collected five ¹⁴C samples from the Suyukou scarps (see section 5.1 for sample locations). The samples were dated at the Oxford Radiocarbon Accelerator Unit (ORAU) at the Research Laboratory for Archaeology and the History of Art (RLAHA). Details of the methods used during sample preparation can be found in *Bronk et al.* [2004] and *Brock et al.* [2010]. Ages were then calibrated using version 4.2.4 of the OxCal program [*Bronk Ramsey and Lee*, 2013] applying the atmospheric curve of *Reimer et al.* [2013]. Calibrated radiocarbon ages are given in Table 1.

4.2. DEM Construction and DEM Resolution

We constructed an high-resolution DEM of the East Helanshan Fault from five stereo pairs of Pleiades images that were acquired on 23 April, 17 July, 24 July, and 25 July 2014. The images were processed using the Leica Photogrammetry Suite module of the ERDAS Imagine software [*Parsons et al.*, 2014; *Zhou et al.*, 2015]. Tie points were used to compensate for the orientation errors in the original rational polynomial function (RPF) sensor model that approximates the relationship between image and ground coordinate systems. Having refined the RPF model, a pixel-by-pixel matching procedure was implemented with a window size of 9-by-9 pixels and a correlation coefficient of 0.3 to 0.7. Other parameters were tried, but this combination was found to give a good balance between point density and topographic smoothing. The apparent offset of a given point on the ground between the two images was then triangulated in order to determine the three-dimensional position of that point. The resulting point cloud from pairwise matching was filtered by averaging within a block of 1 m and then gridded with a pixel spacing of 1 m (using the WGS84 ellipsoid and the UTM 48 N coordinate system) using continuous curvature splines in tension and a tension factor of 0.75. The imagery was then orthorectified using the Pleiades DEM. The final hill-shaded DEM is shown in Figure 3a.

Figures 4a and 4b display statistics for the whole of the Pleiades DEM. When gridded on 1 m by 1 m grid cells, 48% of cells contain at least one point; with 2 m by 2 m cells, 68% of cells contain at least one point. Figures 4c and 4d show similar statistics for a 200 m wide polygon that follows the trace of the scarp. Within this polygon, 60% of 1 m by 1 m grid cells and 79% of 2 m by 2 m grid cells contain at least one point. However, for the Suyukou section of the DEM, 17% of 1 m by 1 m grid cells and 34% of 2 m by 2 m grid cells contain at least one point (see Figures 4e and 4f). Figure 4g shows an example of part of the point cloud on the Suyukou scarps;

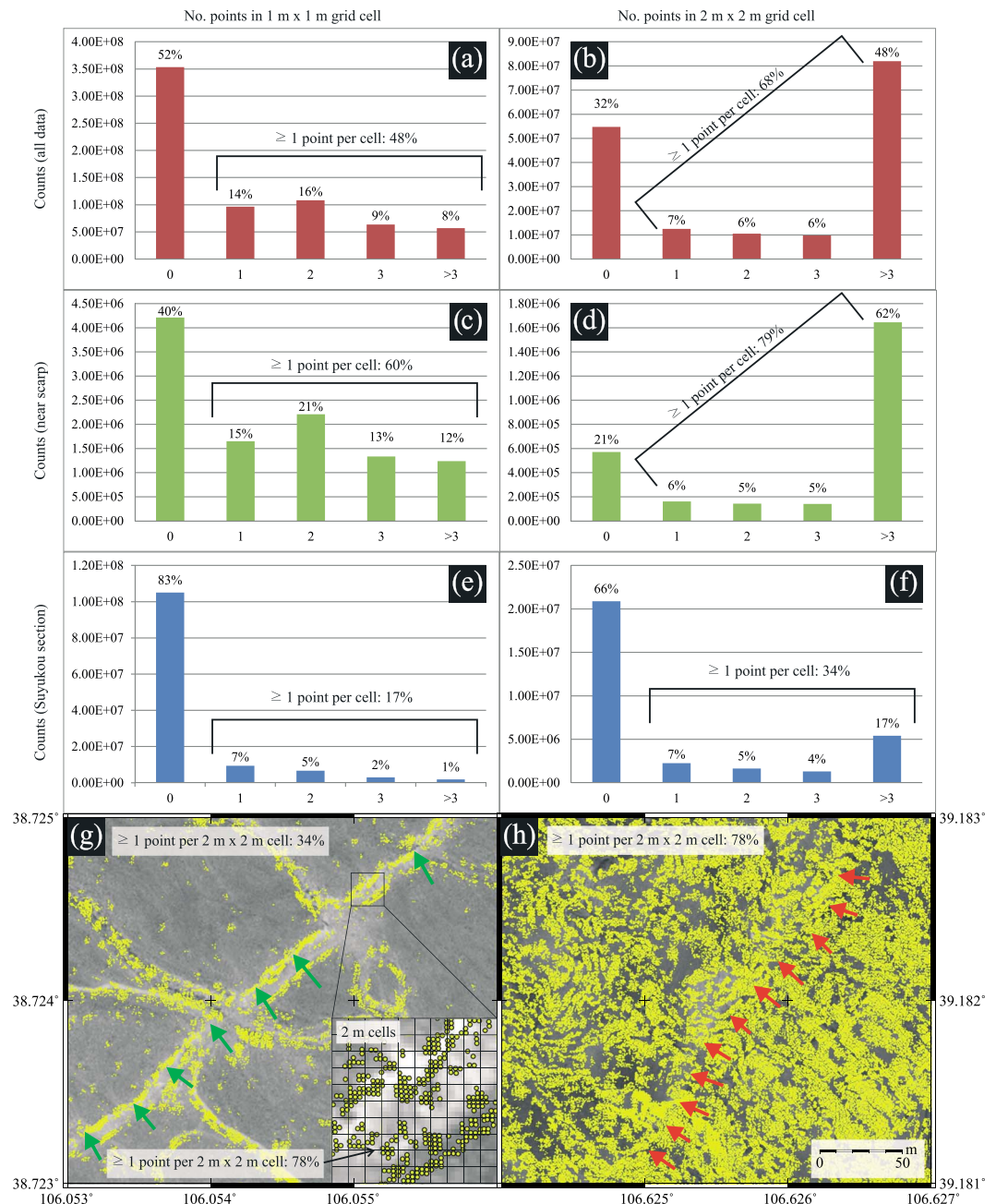


Figure 4. (a) Statistics for the whole DEM when gridded on 1 m by 1 m cells. (b) Statistics for the whole DEM when gridded on 2 m by 2 m cells. (c) Statistics for an approximately 200 m wide swath around the scarp when gridded on 1 m by 1 m cells. (d) Statistics for an approximately 200 m wide swath around the scarp when gridded on 2 m by 2 m cells. (e) Statistics for the Suyukou section of the DEM when gridded on 1 m by 1 m cells. (f) Statistics for the Suyukou section of the DEM when gridded on 2 m by 2 m cells. (g) Pleiades imagery and raw point cloud for part of the Suyukou section of the DEM. Compound scarps are marked by green arrows. Zoomed view shows that in the region around the scarp 78% of 2 m by 2 m grid cells contain at least one point. (h) Pleiades imagery and raw point cloud for part of the Hongguozigou section of the DEM, at the same scale as Figure 4g. Single-event scarps are marked by red arrows.

Table 2. Vertical Offset Measurements From the Pleiades DEM

Profile Number	Distance Along Strike (km)	Local Fault Strike (deg)	Swath Width (m)	Slope Difference ^a (deg)	Vertical Offset (m)	RMS Residual (m)
1	0.65	23	20.7	1.0	2.0	0.5
2	0.95	40	20.4	0.3	0.4	0.6
3	1.25	18	19.8	−0.1	2.8	0.5
SD16 ^b	2.12	−10	n/a	n/a	2.7	n/a
SD15 ^b	2.22	1	n/a	n/a	3.2	n/a
4	2.43	33	20.8	−0.6	4.3	0.6
5	2.91	41	20.1	0.9	2.1	0.7
8	6.27	46	14.9	0.9	2.9	0.5
SD27 ^b	6.37	44	n/a	n/a	3.1	n/a
SD28 ^b	6.47	38	n/a	n/a	3.3	n/a
9	6.48	45	10.3	−0.2	2.7	0.6
11	10.79	47	20.3	−0.3	2.7	0.8
SD50 ^b	10.85	44	n/a	n/a	4.4	n/a
13	11.31	42	20.4	−0.4	3.2	0.5
SD54 ^b	11.46	47	n/a	n/a	3.9	n/a
14	11.49	49	20.1	−1.0	5.1	0.8
SD55 ^b	11.70	36	n/a	n/a	3.0	n/a
15	11.71	41	17.8	−0.2	1.8	0.5
16	11.83	51	20.2	−0.2	2.4	0.6
SD56 ^b	12.00	51	n/a	n/a	3.4	n/a
18	12.12	61	20.9	0.8	2.9	1.3
SD58 ^b	12.18	54	n/a	n/a	2.0	n/a
19	12.32	103	20.1	−0.4	1.2	0.6
SD61 ^b	12.70	34	n/a	n/a	1.2	n/a
20	12.79	38	20.6	−0.6	1.4	0.7
21	13.92	48	20.1	0.2	1.8	0.7
23	14.28	12	20.2	−0.1	1.0	0.6
24 + 25 ^c	14.53	49	n/a	n/a	3.3	1.2
26	16.73	33	20.3	−1.0	2.5	0.9
27	17.21	63	20.8	−0.8	1.4	0.6
28	18.03	42	20.1	0.1	2.0	0.5
29	18.62	53	20.9	0.4	1.0	0.5
30	18.87	27	20.5	−0.4	3.3	0.6
31	21.18	70	20.0	−0.2	4.3	0.5
33	22.13	54	20.6	−0.4	2.3	0.8
36	28.39	36	10.6	−0.3	3.0	0.5
38	32.27	41	20.3	0.9	4.9	0.7
43	58.27	50	20.4	0.8	3.9	0.8
46	60.85	92	10.3	−0.3	1.2	0.5
47	61.31	49	10.4	−0.5	1.5	0.5
51	73.39	91	10.6	0.0	2.4	0.4
53	73.52	101	10.2	−0.5	2.7	0.3
55	73.92	35	10.5	−0.3	4.7	0.5
56	74.23	31	10.5	0.1	4.1	0.6
58	74.71	60	10.2	−0.2	3.6	0.5
59 + 60 ^c	75.14	52	n/a	n/a	4.7	0.7
61	75.99	73	10.3	0.4	3.2	0.6

Table 2. (continued).

Profile Number	Distance Along Strike (km)	Local Fault Strike (deg)	Swath Width (m)	Slope Difference ^a (deg)	Vertical Offset (m)	RMS Residual (m)
HD717-2 ^b	80.86	62	n/a	n/a	1.1	n/a
HD717-3 ^b	81.12	82	n/a	n/a	1.2	n/a
64	81.36	44	10.5	−0.4	3.7	0.5
65	81.64	26	10.4	−0.6	2.2	0.4
66	81.91	66	10.2	−0.7	3.7	0.5
71	82.87	38	10.0	0.4	1.4	0.6

^aDifference in slope between regression lines fitted to the point cloud data above and below the scarp.

^bIdentification code used by *Deng and Liao* [1996]; SD refers to Suyukou and HD to Hongguozigou.

^cProfiles from two parallel fault strands added together.

Figure 4h shows part of the point cloud on the Hongguozigou scarps at the same scale. It is thought that the significantly less dense point cloud on the Suyukou section is due to the large proportion of this region (more than 50%) that is covered by flat, featureless alluvial fans. However, the zoom in Figure 4g indicates that adjacent to the scarp 78% of 2 m by 2 m grid cells contain at least one point, which is similar to the resolution achieved in other sections of the DEM. Therefore, for the regions we are interested in, the Pleiades DEM has an horizontal resolution of between 1 and 2 m.

4.3. Measurement of Topographic Profiles

A number of topographic profiles and vertical offset measurements across the scarp are presented in sections 5.2, 6.2.1, and 6.2.2. These measurements were made on the high-resolution Pleiades DEM at locations where we identified a single-event scarp (see section 4.4). The offset measurements were made on the raw Pleiades point cloud by taking swath profiles, perpendicular to the local fault trace, which were 10 to

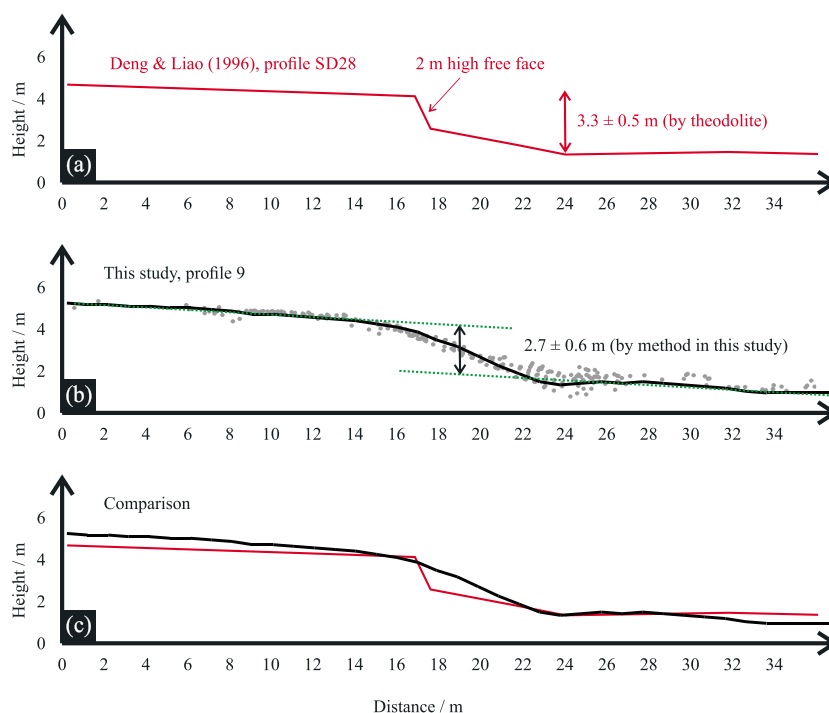


Figure 5. (a) Profile SD28 from *Deng and Liao* [1996] measured by theodolite. This profile is measured at the location marked p9 in Figure 7b. *Deng and Liao* [1996] record a vertical offset of 3.3 m and a 2 m high free face. We estimate an error of ± 0.5 m on their offset measurement. Note that there is no vertical exaggeration on this plot. (b) Profile 9 from this study measured from the Pleiades DEM at the same location and displayed at the same scale. Black line shows single profile and grey points show data from within the swath that was used to obtain our vertical offset measurement of 2.7 ± 0.6 m using the method described in section 4. Note that we used a 250 m long profile for this measurement and only the central section is shown here. (c) Comparison of the two profiles.

20 m wide and at least 100 m long and then projecting all points within this swath onto a line. Separate straight lines were fitted to the heights above the scarp and those below the scarp with a simple least squares regression. Using the optical imagery to help identify unmodified fan surfaces, the data to fit were selected by hand, being careful to avoid vegetation and eroded channels. If the slope of the two lines differed by 1° or more, the profile was discarded since it was deemed not possible to adequately match the upper and lower surfaces in such cases. For the remaining profiles, parallel straight lines were then fitted to the data above and below the scarp in order to measure the vertical offset. The root-mean-square (RMS) residual in fitting these lines was then taken as the error on the offset measurement. Also, on the basis of our scarp mapping (see section 4.4), we estimated the local fault strike at each location where a vertical offset measurement had been made. We assumed a typical error of $\pm 5^\circ$ on each of these estimates of fault strike. In total, measurements were made at 41 sites and then combined with field data from Suyukou and Honggouzigou by *Deng and Liao* [1996] to give a complete suite of 53 measurements. All of these data are given in Table 2.

In order to assess the reliability of topographic profiles measured on the Pleiades DEM we compared one of our measurements to a theodolite profile from the same location measured in the field by *Deng and Liao* [1996] (see Figure 5a). In Figure 5b the grey circles show all of the points from within the swath that were used to make the offset measurement, while the black line shows a simple profile from the center of the swath. Note that in profiles on subsequent figures we have not shown the grey points, even though this data was used to make all of the offset measurements that we quote. Figure 5c indicates that the steepness of the free face is not entirely captured by the Pleiades DEM, but that the vertical offset measured according to our method agrees with the field measurement to within their stated errors.

Additionally, we tested the effect of using different swath widths. At the location of profile 53 (marked B-B' in Figure 16b), we tried swath widths of between 5 m and 40 m (in increments of 5 m) and the measured offset varied by less than 0.2 m between all eight measurements. Meanwhile, the estimated error increased from ± 0.3 m for the 5 m swath to ± 0.6 m for the 40 m wide swath. This indicates that our approach of taking a single 10 to 20 m wide swath at each measurement site is appropriate for obtaining a set of offset measurements that allow us to investigate larger-scale changes in throw along strike.

4.4. Scarp Mapping and Type Locality Calibration

Previous authors have strongly suggested that the Suyukou scarps were produced in the 1739 earthquake [*Zhang et al.*, 1982; *Deng et al.*, 1984; *Zhang et al.*, 1986; *Deng and Liao*, 1996; *Bai and Jiao*, 2005]. Here we describe the morphology of the Suyukou scarps in detail and how they show up on the Pleiades DEM. We then use these observations to inform our mapping of the other scarps along the East Helanshan Fault.

The Suyukou scarps vary in strike between about 10° and 50° , cutting through a series of four, large, coalesced, alluvial fans [*Deng and Liao*, 1996]. The fan material is unconsolidated and very coarse, comprising subangular gravel, cobbles and boulders (see Figure 6c and inset in Figure 7a). A 2 to 3 m high free face, with a dip of between 70° and 90° , exists along approximately 70% of the Suyukou scarps [*Zhang et al.*, 1986]. *Zhang et al.* [1986] also considered how the free face has been degraded and found that it has largely disappeared on scarps less than 2 m high (though the rate of erosion is also likely to depend on the properties of the footwall material). In many sections the free face rides on a cumulative scarp, but in some locations, adjacent to active river channels, a fresh, single-event scarp is visible. On the compound scarps, a distinct bevel separates the free face from the top of the scarp and a debris slope, with a 30° angle of repose, is common below the free face. In some places, the scarp has been eroded by episodic gully incision, depositing secondary splay fans on the hanging wall side. The predominant wind direction is from the west, resulting in significant accumulations of aeolian loess in the lee of the scarp.

On the Pleiades DEM, the Suyukou scarps appear as sharp topographic discontinuities. We were not able to resolve the free face (see section 4.3), but having observed it during our field reconnaissance in a number of locations, we were then able to trace it along strike in the DEM. A slope map derived from the Pleiades DEM was also used to help distinguish between freshly ruptured and older scarps. Scarps that had shown a free face in the field had typical slopes of 30 to 45° on the DEM, whereas scarps with no free face had typical slopes of 20 to 25° .

In the Pleiades DEM and imagery, compound scarps could be distinguished from single-event scarps by the relative width of the scarp (see Figure 7c). We were also able to identify terrace risers (using both the DEM and the slope map), which allowed us to differentiate single-event scarps bordering the youngest surface from

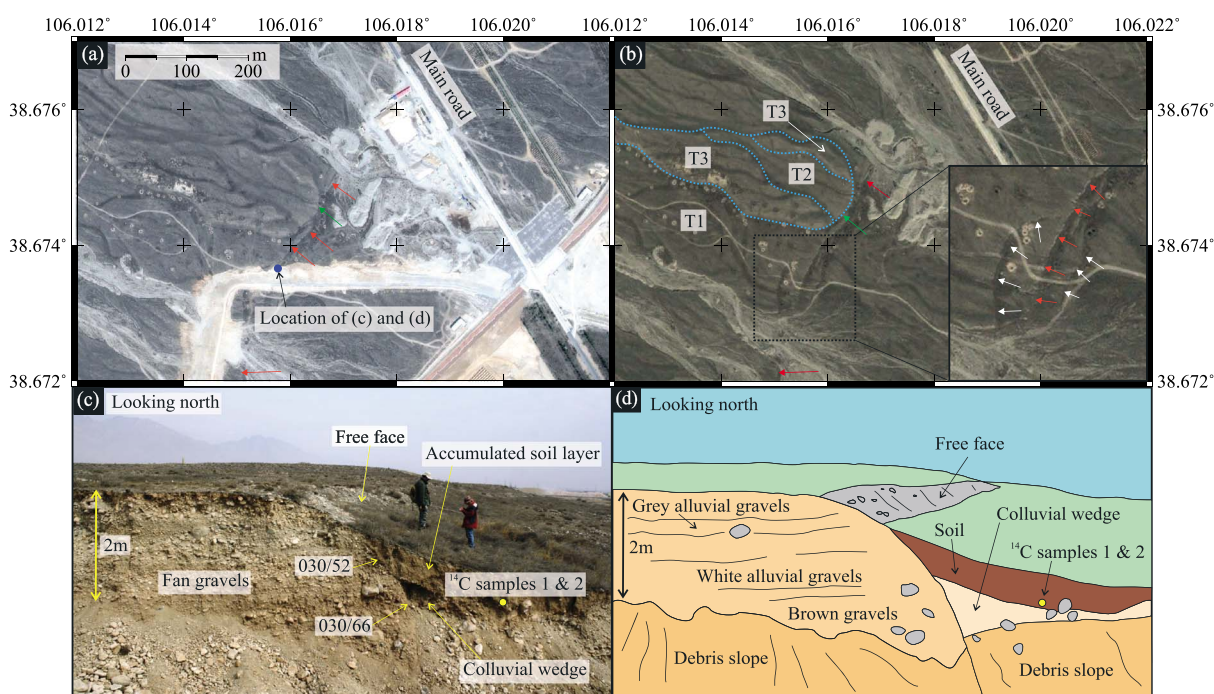


Figure 6. (a) Pleiades imagery of a road-cut exposure through the Suyukou scarps. Single-event scarps are marked by red arrows; compound scarps are marked by green arrows. (b) Google Earth imagery from September 2012 (source: <http://earth.google.com>) of the same location at the same scale prior to the building of the road. Three terrace levels, outlined in blue, are identifiable in the footwall of the fault. Zoomed image shows three separate fault strands. Main strand marked by red arrows and subsidiary strands marked by white arrows. The total throw across all three strands is 4.3 m. (c) Annotated field photograph (taken at 38.674°N, 106.016°E) showing a cross section through the main fault strand at the road-cut exposure. Yellow circle indicates the location of ^{14}C samples 1 and 2 for dating the accumulated postearthquake soil. (d) Sketch of the same view as in Figure 6c indicating the principal units exposed in this section.

compound scarps bordering the older surfaces. Also, knowing that the maximum single-event, vertical offset from the places visited by Zhang *et al.* [1986] and Deng and Liao [1996] was around 4 to 5 m, we were able to classify any scarps more than 10 m high as compound scarps. Scarps that were 5 to 10 m in height were only classified as single-event scarps if we were able to verify in the field that they showed a single free face and no bevel at the top of the scarp.

This said, differentiating between the different generations of scarps was not always straightforward, and to some degree the results are subjective—there were also some scarps that we were not able to classify. The resulting map is shown in Figure 3b. We discuss the main features of this map in section 5.2.

5. Results

5.1. Palaeoseismological Work on the East Helanshan Fault

We took samples for ^{14}C analysis at three locations along the Suyukou scarps, as described below.

5.1.1. Road-Cut Exposure

Our first sample site was at the southernmost end of the Suyukou scarps (38.674°N, 106.016°E), 360 m southwest of the road leading from Yinchuan to the range front (see Figure 3 for location). Major, industrial landscape modification is taking place at this site and when we visited in March 2014 a new road excavation had just been cut through the scarp (see Figure 6). At this location the fault forms a braided pattern with at least two subsidiary scarps (see Figure 6b). The total throw across all three scarps, measured on the Pleiades DEM, is 4.3 m. The road cutting exposes a cross section of the main scarp with its preserved free face (see Figure 6c). The scarp footwall is composed of subhorizontal deposits of unconsolidated, subangular fan gravels. Clasts range in size from sand grade to 10 or 20 cm in diameter. The same gravels are just visible in the exposed parts of the hanging wall, enabling us to measure a fault slip on the central strand of 3.95 m. We also recorded a surface fault dip of 66°, shallowing to 52° near the eroded top of the scarp. (This is in agreement with the surface fault dip measurements made in nearby trenches by Deng and Liao [1996], which varied between 65° and 85°, but is substantially different to the 39° fault dip at depth suggested by the seismic

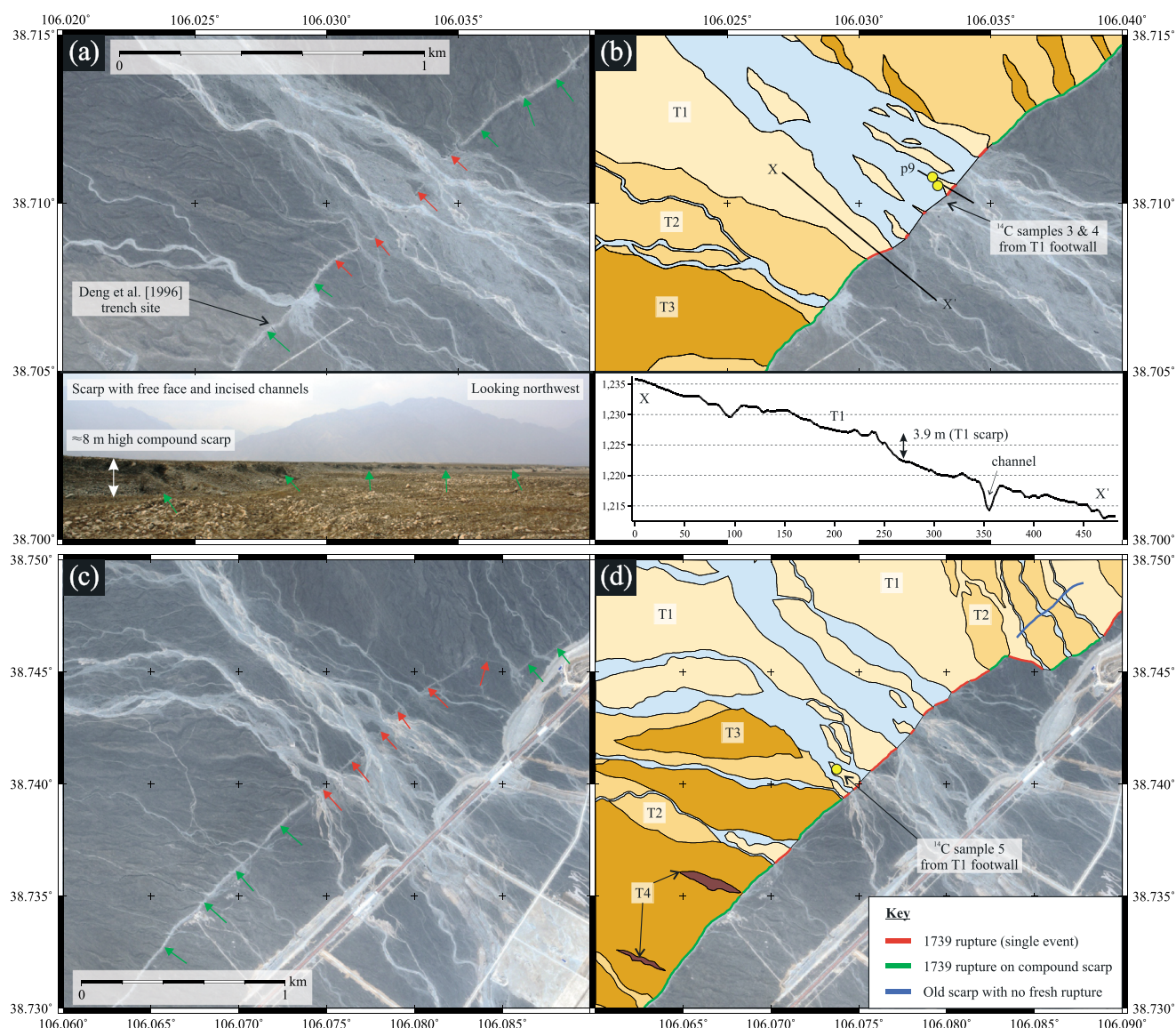


Figure 7. (a) Pleiades imagery of a major river crossing the Suyukou scarps at 38.710°N, 106.033°E. Single-event scarps are marked by red arrows; compound scarps are marked by green arrows. Inset photograph shows free face preserved on many of the scarps. (b) Annotated geomorphological map of the same site, showing different generations of alluvial fan surfaces. The inset profile indicates a typical scarp height for the youngest terrace (T1). Fault scarps are mapped in red, green and blue according to the key. Yellow circles indicate ¹⁴C samples 3 and 4 taken from the uplifted terrace material in the immediate footwall. p9 indicates another profile, shown in Figure 5. (c and d) Another river crossing site on the Suyukou scarps at 38.741°N, 106.075°E with similar annotations. ¹⁴C sample 5 was taken here.

profile in Fang *et al.* [2009]—see also Figure 2b.) Together, the 3.95 m slip and 66° dip suggest a vertical off-set on the central strand of 3.6 m, which is consistent with the total throw of 4.3 m across all three strands. (We do not have estimates of slip on the other two strands.) The hanging wall gravels are covered by a colluvial wedge, also composed of fan gravels though with noticeably less consistent clast orientations and even poorer consolidation. The colluvial wedge is overlain by a 70 cm thick layer of brown soil, sand, and loess. ¹⁴C samples 1 and 2 (both faecal pellets) were taken from within this postearthquake soil between 60 and 70 cm below the ground surface (see Figures 6c and 6d). Both samples from the road-cut exposure returned modern ages (see Table 1).

5.1.2. First River Exposure

The second sample site was at 38.710°N, 106.033°E, where a major braided river channel from the Helanshan crosses the Suyukou scarps. On the footwall side a stepped series of river terraces has been preserved adjacent to the channel that may correspond to a sequence of earthquakes at this location [Deng and Liao, 1996].

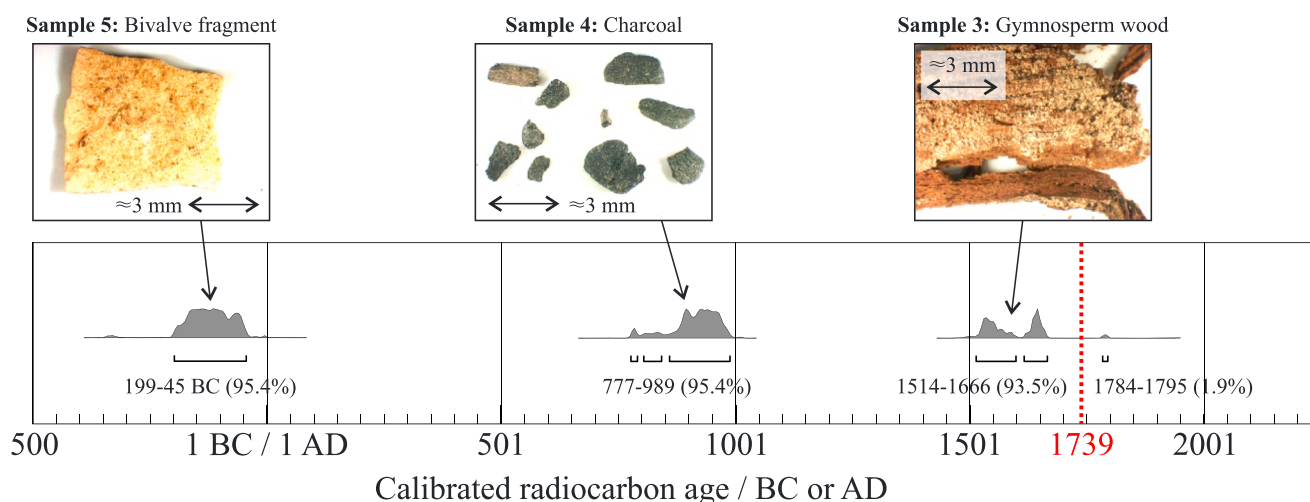


Figure 8. Time line showing the calibrated radiocarbon ages of ^{14}C samples 3, 4 and 5 from the T1 terrace (locations shown in Figures 7b and 7d). Grey histograms show normalized probability density functions, indicating the range of possible ages for each sample within certain percentage confidence limits. All three samples predate 1739.

The lowest terrace (T1), which is interpreted to represent the most recent earthquake, is typically around 3 m above the hanging wall level. Remnant islands of this surface that have not yet been completely removed by fluvial erosion are also visible within the main channel itself, further supporting the idea that they represent a relatively young, single-event scarp (see Figures 7a and 7b). The footwall material here is similar to that seen at the road-cut site, though with a slightly larger proportion of finer clasts; in places the gravel layers are interbedded with fluvial sands and silts. ^{14}C samples 3 and 4 were taken from the exposed side of one of the T1 islands within the river and hence from the immediate footwall of the fault (see Figure 7b). Sample 3 was a piece of gymnosperm wood from a fluvial sand layer approximately 70 cm below the ground surface. This sand layer was overlain by a 60 cm thick unit of poorly sorted, subangular alluvial gravels and around 10 cm of soil development. Sample 4 was a fleck of charcoal from a sand lens 80 cm below the ground surface. It was also overlain by a single unit of poorly sorted, subangular alluvial gravels. Sample 3 returned a calibrated radiocarbon date of 1514 to 1795 AD (95.4% probability, i.e., within two standard deviations of the mean), and sample 4 returned a calibrated radiocarbon date of 777 to 989 AD (95.4% probability). These ages are shown in Figure 8 and Table 1.

5.1.3. Second River Exposure

The final sample site was at 38.741°N , 106.075°E , where another major river from the Helanshan crosses and dissects the Suyukou scarps (see Figures 7c and 7d). The geomorphology is very similar to that at the first river exposure (see section 5.1.2). ^{14}C sample 5, a single fragment of bivalve shell, was taken from the side of the T1 surface on the footwall side at a depth of 40 cm (see Figure 7d). The sample came from within a 50 cm thick layer of yellow-brown sand and silt overlain by 10 cm of rounded gravels. Sample 5 returned a calibrated radiocarbon date of 199 to 45 BC (95.4% probability). The age result is also shown in Figure 8 and Table 1.

5.1.4. Interpretation of Dating Results

All three footwall samples predate 1739. The only possible exception is that, within the two standard deviation range, there is a very small probability (1.9%) that sample 3 is younger than 1739 (see Figure 8). Nonetheless, taken together, the samples indicate that the material preserved in the T1 terrace was almost certainly deposited prior to 1666 (the limiting age of sample 3 for a probability of 93.5%). Combined with the modern ages for the postearthquake soil at the road-cut site, we therefore have strong evidence that the uplift of T1 has occurred between 1666 and the present day. The only recorded earthquake of any significant magnitude ($M_w > 5$) in this time frame and at this location is the 1739 event. We therefore conclude that the 1739 Yinchuan earthquake occurred on the East Helanshan Fault.

5.2. Geomorphology of the 1739 Rupture

We mapped an end-to-end rupture length of 87 km (see Figure 3b). The ends of the rupture were verified in the field; although the fault continues to both the north and the south, there are no signs of recent surface displacement in the form of a free face or similar at, for example, 39.262°N , 106.671°E in the north and 38.540°N , 105.986°E in the south. Although the ends of the named segments (Suyukou, Xiashigou, Jianquan and

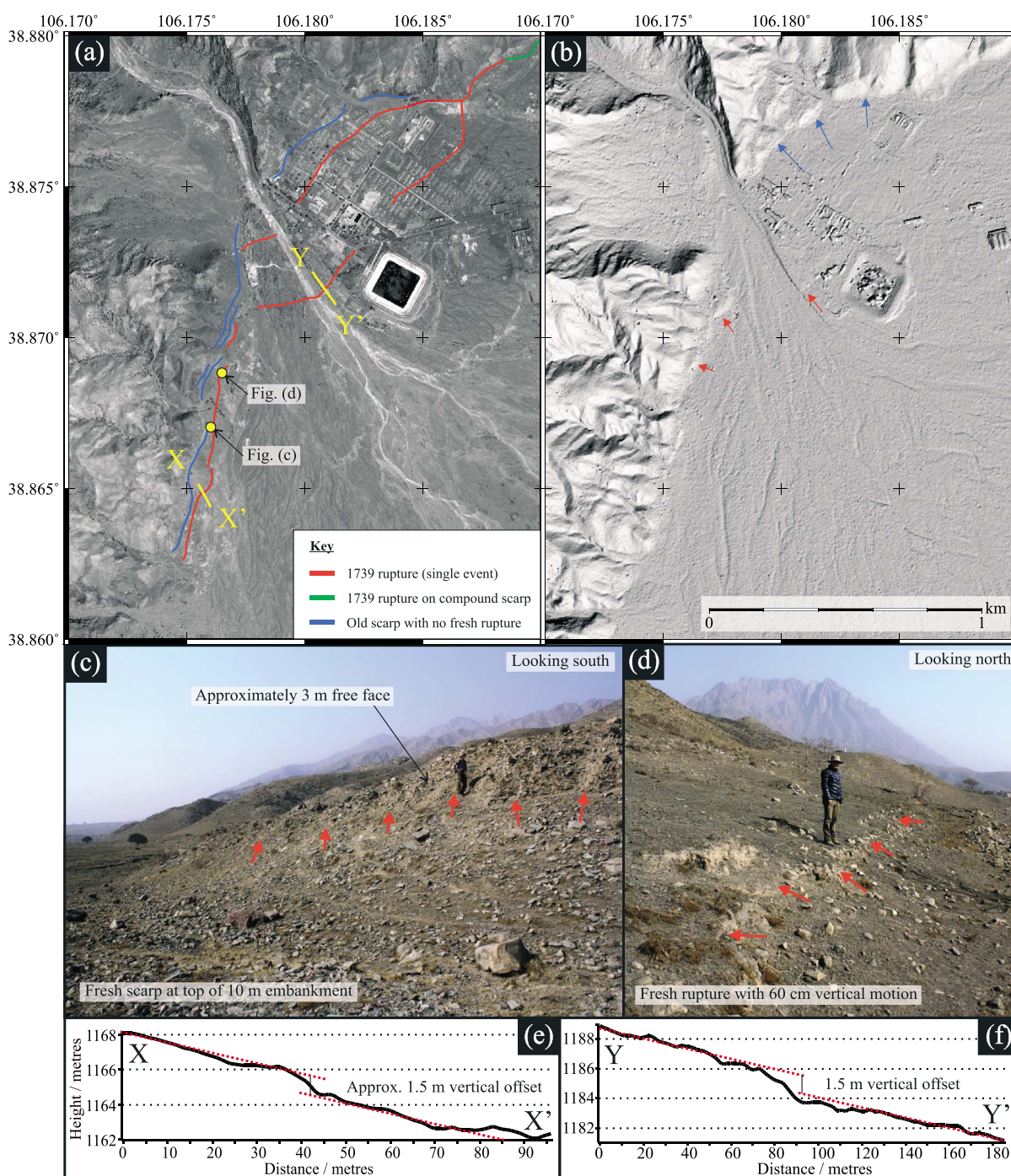


Figure 9. (a) Pleiades imagery of the Xiashigou portion of the East Helanshan Fault. Fault scarps are mapped in red, green and blue according to the key. Yellow dots indicate sites visited in the field and shown in Figures 9c and 9d. (b) Pleiades DEM of the same region as Figure 9a. Red arrows indicate places where the 1739 rupture is particularly clear on the DEM; blue arrows point to an older, smoother, compound scarp. (c and d) Field photographs from 38.867°N, 106.176°E and 38.869°N, 106.176°E showing evidence for a fresh rupture and its associated free face in alluvial gravels on the Xiashigou segment. (e and f) Topographic profiles from the Pleiades DEM at the locations marked in Figure 9a showing the vertical offset at two other locations on the Xiashigou segment.

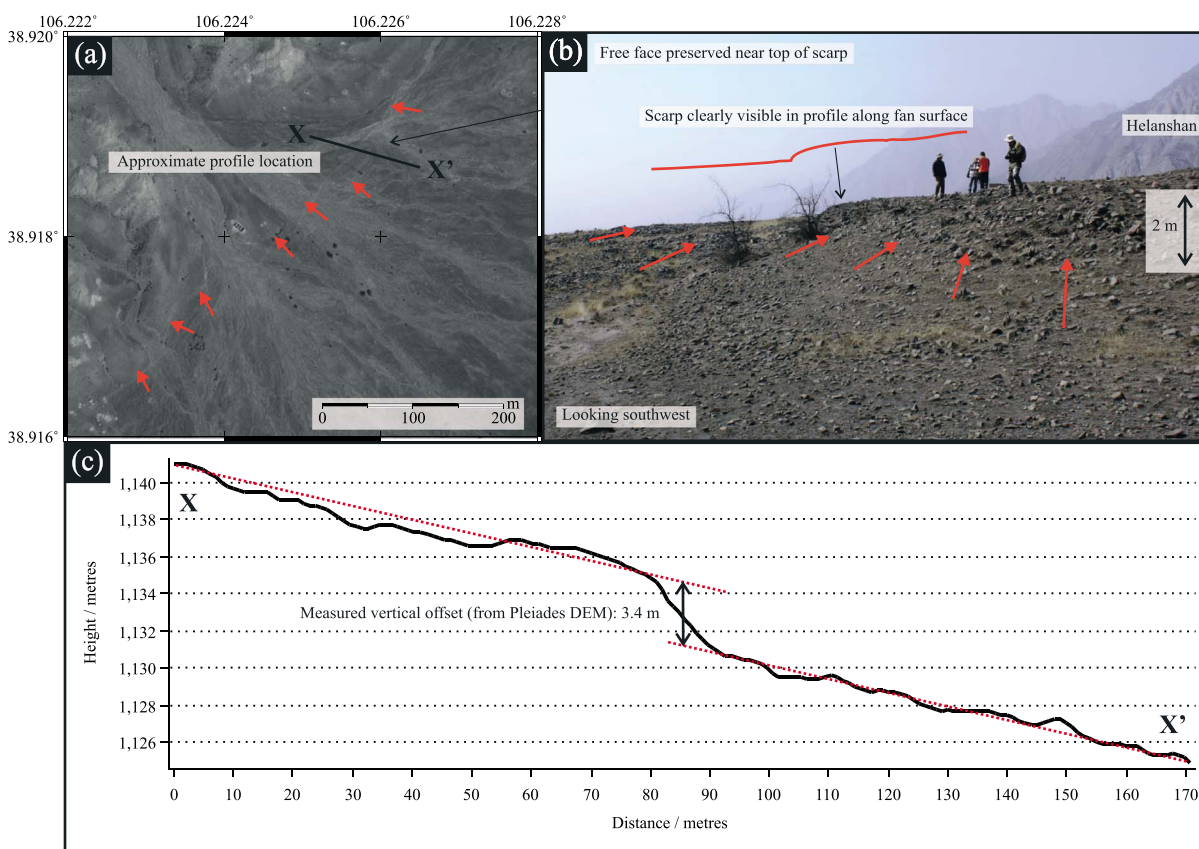


Figure 10. (a) Pleiades imagery of part of the Xiashigou segment of the East Helanshan Fault. The location of the 1739 rupture trace is indicated by red arrows. (b) Field photograph taken at 38.919°N, 106.226°E showing the 1739 rupture and the characteristic free face. (c) Topographic profile from the Pleiades DEM at the location marked in Figure 10a showing a vertical offset at this location of 3.4 m.

Hongguozigou) correspond to geometrical discontinuities along the fault, we do not presuppose any knowledge of kinematic segmentation; the names are merely convenient shorthand for referring to different portions of the fault.

We also identified two step over zones: one of about 4 km between the end of the Suyukou segment and the start of the Xiashigou segment and the other of around 2 km in the middle of the Jianquan segment (see Figure 3). We note that the first of these step overs is accompanied by a number of subparallel scarps on the intervening relay ramp, at least some of which ruptured in 1739. The second step over occurs at a sharp bend in the range front, and it is unclear as to whether or not these segments are linked at depth. Additionally, we observe that the rupture trace is not simple: it is corrugated, with considerable changes in local fault strike of up to 70°. In a number of locations there also appear to be multiple active strands. The fault geometry will be discussed further in section 6.2.2, but we note here that such a complex rupture pattern is not unexpected; the M_s 6.8 1954 Dixie Valley earthquake in western Nevada, for example, displayed a similar pattern [Caskey *et al.*, 1996].

5.2.1. Xiashigou

Figure 9 shows part of the Xiashigou segment at the location first identified by Deng and Liao [1996] (see Figure 3 for location). Here a series of scarps are apparent adjacent to the range front. The Pleiades DEM and Google Earth imagery also show evidence for two fresher rupture strands that diverge from the range front. Figures 9c and 9d show field photographs from two locations on the Xiashigou segment. At both of these locations a free face was observed, indicating that the scarp seen in the DEM is from 1739 (according to the criteria set out in section 4.4). The topographic profiles in Figures 9e and 9f both show a vertical offset of 1.5 m, which is consistent with the previous measurements of 1 to 2 m made by Deng and Liao [1996]. However, the photographs in Figures 9c and 9d show scarp heights (measured in the field) of 3 m and 0.6 m, respectively. These heights were measured vertically from the proximal hanging wall, so it is to be expected that they differ from the nearby topographic profiles where alluvial surfaces were fitted over an horizontal

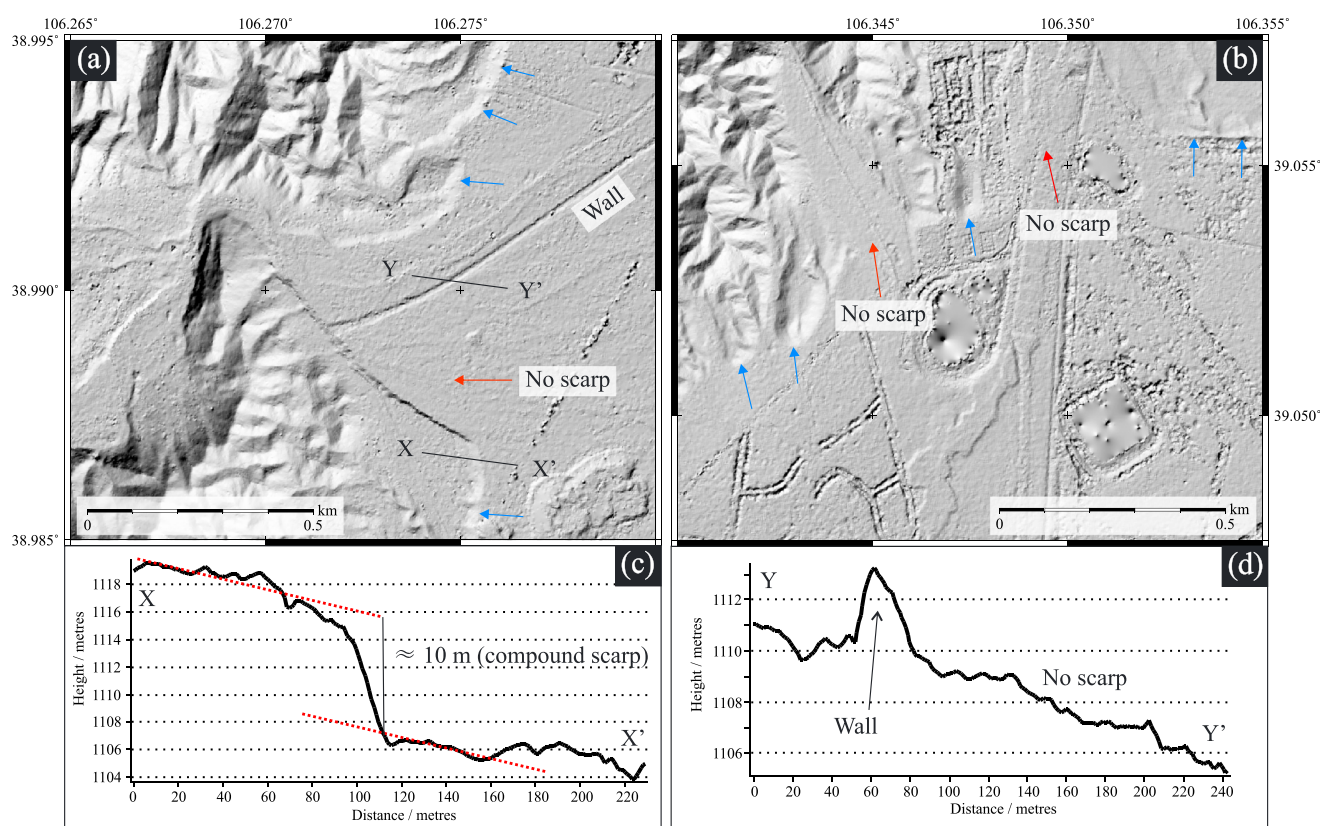


Figure 11. (a) Zoomed in view of the Pleiades DEM at the range front northwest of Shizuishan city. Blue arrows highlight an old (compound) fault scarp. The undisturbed alluvial material highlighted by the red arrow suggests that the 1739 earthquake did not rupture this portion of the range front. (b) Similar DEM view from a location just to the north, also indicating a lack of fresh rupture on this portion of the range front. (c) Topographic profile X-X' across the compound scarp. (d) Topographic profile Y-Y' across the undisturbed alluvial material.

distance of 100 m or more. It is also likely that there is some variability in the geomorphological expression of the fault along strike over relatively short distances.

Figure 10 also shows part of the Xiashigou segment (see Figure 3 for location). Again, a free face was seen in the field and the scarp can be followed across an alluvial fan in the Pleiades imagery. At this site we measured a vertical offset of 3.4 m from the Pleiades DEM. The fresh scarps can be followed almost continuously from the location of Figure 9 to the location of Figure 10 except for a few short sections where the scarps have been eroded or obscured by human activity.

5.2.2. Shizuishan City

No fresh scarps were identified in the Pleiades DEM for a length of approximately 15 km between the Xiashigou and Jianquan segments, a region where the range front is embayed and the intervening land is largely covered by Shizuishan city (see Figure 3). This includes both the Helanshan range front and the alluvial fans to the southeast of the mountains. Figure 11 shows zoomed views of two portions of the Pleiades DEM at the range front behind Shizuishan city (see Figure 3 for locations). In both cases, old compound scarps can be seen with vertical offsets of around 10 m. However, no scarps are visible in the more recent fan sediments immediately abutting channels draining the Helanshan.

5.2.3. Jianquan

Figure 12 shows part of the Jianquan segment, northeast of the step over (see Figure 3 for location). As for the Xiashigou segment (see section 5.2.1), the key piece of evidence for these scarps being from the 1739 event is the observation of a fresh, free face in the field (see Figures 12b and 12e). Along this section, a number of knick points, typically 5 to 7 m high, were observed about 10 m north of the scarp in gullies crossing the fault (see Figures 12c and 12d). If the knick points were from 1739 this would imply a retreat rate of approximately 35 mm/a, but this seems too fast given that these gullies have quite small upstream catchments. Nonetheless, though the knick points are unlikely to be from 1739, they do attest to recent changes in base level across the Jianquan segment of the East Helanshan Fault.

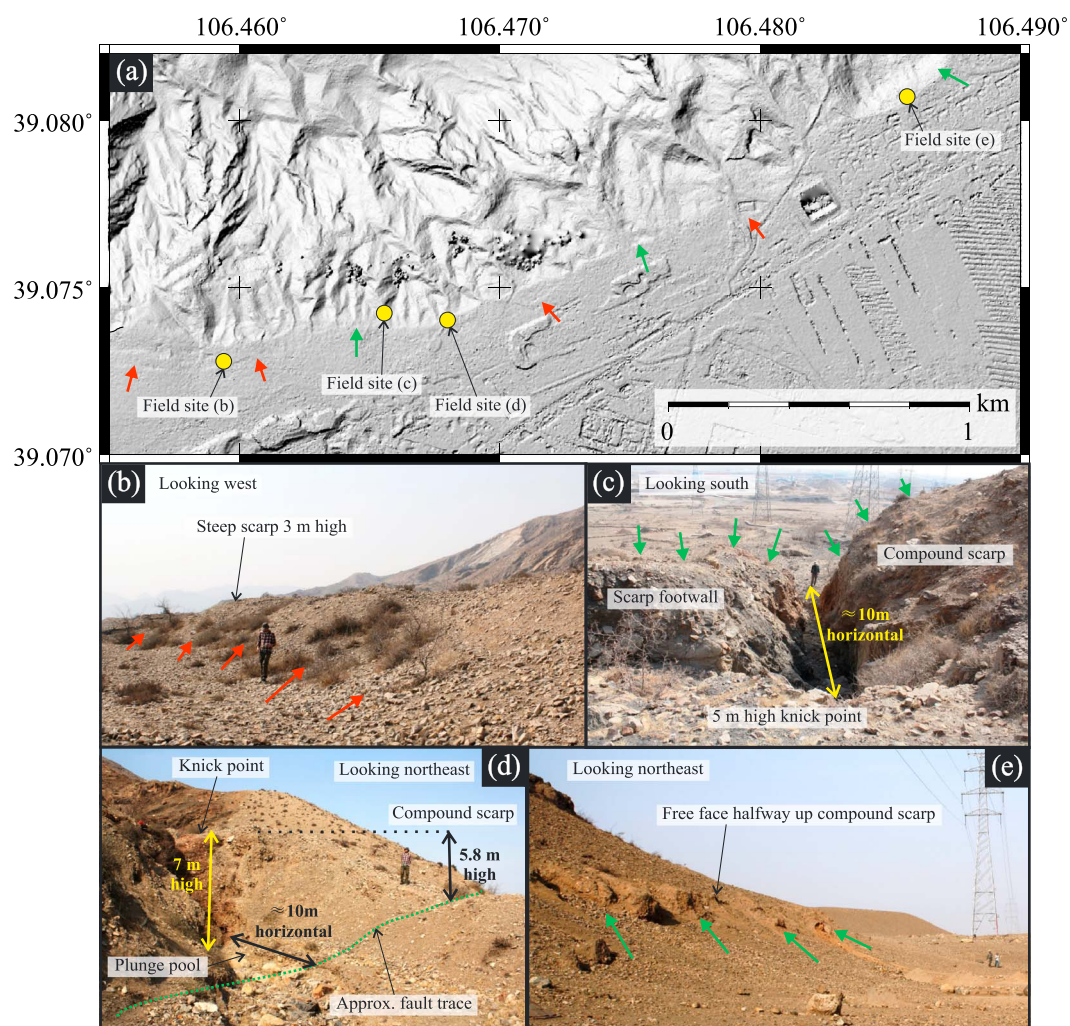


Figure 12. (a) Zoomed in view of the Pleiades DEM at the range front near Jianquan. Single-event scarps are marked by red arrows; compound scarps are marked by green arrows. In some places the rupture steps away from the range front, and an older scarp is visible behind the most recent one. Yellow dots indicate field locations. (b and e) Field photographs (taken at 39.073°N, 106.459°E and 39.081°N, 106.486°E) of the 1739 scarp in alluvial material near Jianquan. (c and d) Field photographs (taken at 39.074°N, 106.466°E and 39.074°N, 106.468°E) of knick points approximately 10 m behind the 1739 scarp at Jianquan.

5.2.4. Hongguozigou

The Hongguozigou segment comprises both the 4 km of scarps near the Great Wall site [Zhang *et al.*, 1986; Deng and Liao, 1996] and a series of fresh-looking scarps, including a near right-angle change in fault strike, identified from the Pleiades DEM (see Figures 3, 13, and 16b and for locations). At the Great Wall site, the fault splits into three strands: the two strands to the northwest dip southeast, while the third is antithetic and dips to the northwest. The Great Wall runs from the southeast to the northwest, crossing all three fault strands before culminating in a beacon stand and a dog-leg to the west in the Helanshan (see Figure 13b). The surrounding area is part of a cemetery, and the geomorphology has been extensively modified by human constructions. A major, recent building project has also covered much of the site (see Google Earth imagery from February 2015 onward).

Original observations of displacement at the Great Wall site were made by Liao and Pan [1982] and Zhang *et al.* [1986]. Zhang *et al.* [1986] measured a cumulative offset across all three fault strands of 2.7 m vertically and 3 m right laterally. They also noted that the northwesternmost strand must be a compound scarp,

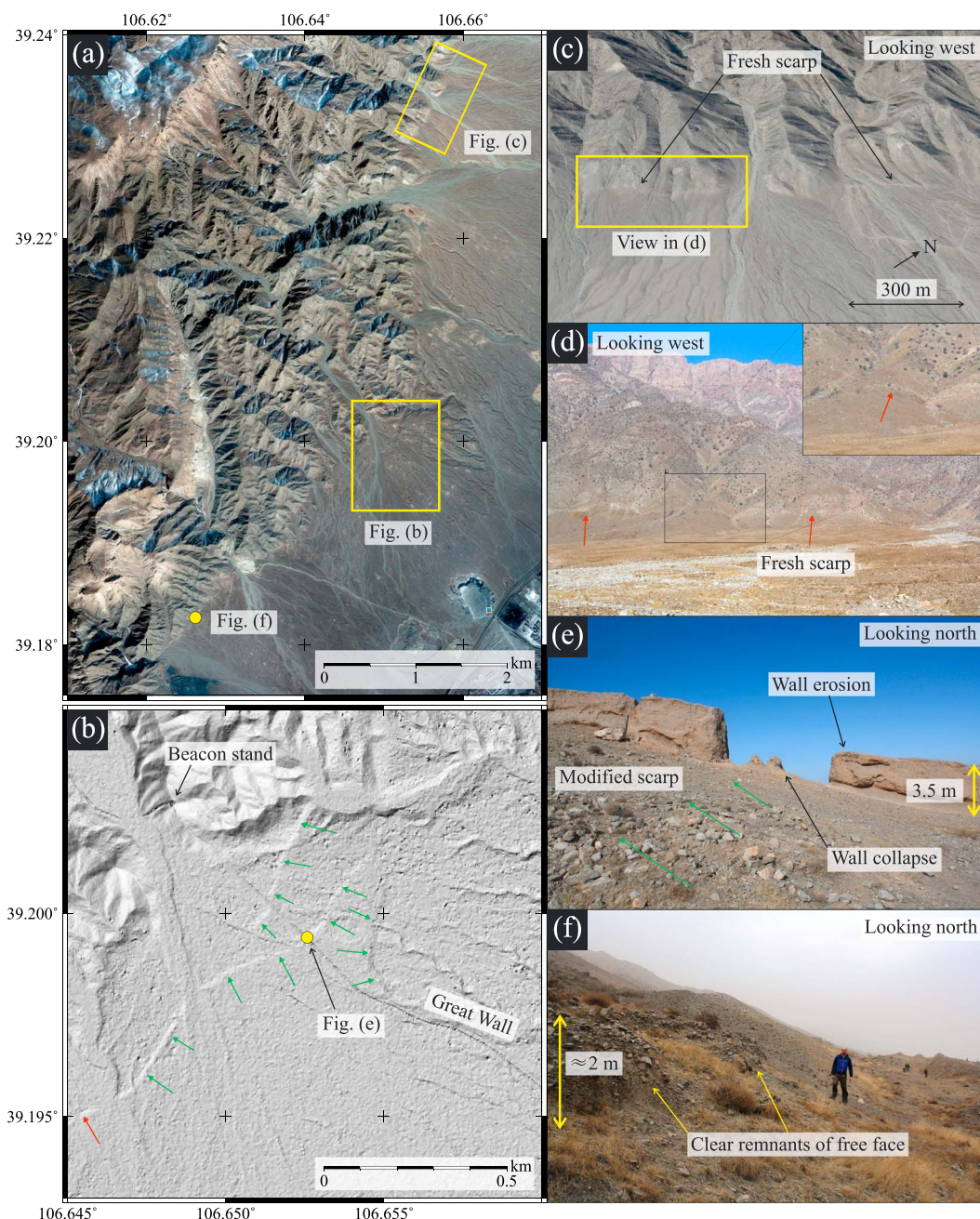


Figure 13. (a) Google Earth imagery from February 2010 (source: <http://earth.google.com>) of the Hongguozigou portion of the East Helanshan Fault toward the northern end of the 1739 rupture. (b) Zoomed-in view of the Pleiades DEM at the Great Wall site. Red arrows indicate single-event fault scarps; green arrows indicate compound scarps. The southeasternmost fault strand is antithetic. (c) Perspective Google Earth view of the range front north of the Great Wall site at the location marked in Figure 13a. (d) Field photograph (taken at 39.073°N, 106.459°E) showing part of the same view as Figure 13c, with clear evidence for a fresh rupture. Zoom shows fresh scarp in more detail. (e) Field photograph (taken at 39.199°N, 106.653°E) of the Great Wall crossing the central strand of the three fault strands shown in Figure 13b. (f) Field photograph (taken at 39.182°N, 106.626°E) of the fault 3 km southwest of the Great Wall site. Remnants of a free face are still visible.

since the scarp height is 3 to 4 m whereas the vertical offset of the wall at this location is only 0.95 m. However, *Lin et al.* [2013] offer a contrasting view and present a detailed argument for why the Great Wall was not offset in the 1739 earthquake.

On the northwesternmost fault strand, we believe that it is not possible to reach any conclusion about the offset because the wall here was rebuilt in the 1980s to include an offset in the new stonework. The only evidence for an offset on this strand is from an unpublished photograph that apparently dates to 1973 [*Zhang et al.*, 1986]. Similarly, we were not able to observe any offsets on the southeasternmost fault strand due to collapse and erosion of the wall. On the central strand, *Lin et al.* [2013] make the case that if you allow for erosion of the wall and follow the lines of adobe bricks within the wall then the bricks are always parallel to the topography, indicating that the wall was built on a preexisting scarp and that there was no dislocation in 1739. However, any reconstructions based on projections and extrapolations of these curved lines of bricks remain equivocal.

Since both the Great Wall and the surrounding fan surface have been so extensively modified we can no longer tell very much from the Great Wall site itself. Nonetheless, there are two key pieces of evidence that lead us to conclude that the rupture did pass through the Great Wall site. First, the wall has collapsed at precisely the location of the scarp on the central fault strand (see Figure 13e). Second and more importantly, we visited sites in the field both to the northeast and to the southwest of the Great Wall site where we found scarps with preserved free faces. In Figures 13c and 13d, 4 km to the north of the Great Wall site, we saw a pale grey band of oversteepening at the base of the Helanshan with preserved portions of free face in alluvial material. A single gully and two boulder ridges also appeared to show evidence of right-lateral motion. Similarly, in Figure 13f, 3 km to the southwest of the Great Wall site, we saw 2 m high remnants of a free face in angular alluvial gravels. We therefore conclude that the 1739 rupture did go through the Great Wall site.

6. Discussion

6.1. The Causative Fault for the 1739 Earthquake

In section 5.1 we showed by way of ^{14}C dating that the formation of the Suyukou scarps can be bracketed to the last 350 years. We also noted that these scarps show a characteristically fresh free face. In section 5.2 we were then able to identify the same scarp morphology at a number of other locations along the East Helanshan Fault (see Figures 9, 10, 12, and 13). This leads us to conclude that the East Helanshan Fault was the causative structure for the 1739 Yinchuan earthquake.

This result is consistent with almost all of the previous palaeoseismological studies in the Yinchuan Graben (see Figure 14). *Lei et al.* [2015] and *Lei et al.* [2008] found from trenching and boreholes on the Yinchuan-Pingluo Fault that the last surface-rupturing earthquake was more than 3400 years ago (as constrained by a ^{14}C date). Given the large magnitude of the 1739 earthquake, it is highly likely that it produced surface ruptures and, therefore, that it did not occur on the Yinchuan-Pingluo Fault. However, we cannot completely rule out the possibility of some subsurface slip on this fault. Similarly, the Luhutai Fault is believed to show no evidence for recent surface ruptures: *Wang et al.* [2007] indicate that the fault is buried under Late Pleistocene sediments from 124 ka ago to a depth of at least 25 m.

Lin et al. [2015] suggested that the 1739 event occurred on the Yellow River Fault (see section 3). However, they were only able to find surface expression of this fault for a length of 8 km. Scaling relationships suggest that the expected surface rupture length of a M_w 7.6 earthquake, for example, would be of the order of 100 km [*Wells and Coppersmith*, 1994]. Although some scarps may have been eroded or covered by migrating dunes from the Ordos Plateau, it seems surprising that no other scarps have been found along the Yellow River Fault if this was the causative structure. Furthermore, *Lei et al.* [2014] found from a composite drilling profile on the northern section of the Yellow River Fault, approximately 25 km southeast of Pingluo, that no earthquakes have occurred here for at least 3625 ± 35 years (^{14}C date). *Wang et al.* [2012] excavated a trench on the Lingwu Fault, the southern extension of the Yellow River Fault, at a location 30 km south-southeast of Yinchuan and found that no earthquakes have occurred on this segment for at least 17.8 ± 0.8 ka (optically stimulated luminescence date).

The trenching work by *Deng and Liao* [1996], *Lin et al.* [2015] and *Lei et al.* [2015] at Suyukou and Hongguozigou is also consistent with the 1739 earthquake taking place on the East Helanshan Fault (see Figure 14 for details). The only data that disagrees with this conclusion are four dates obtained near the Great Wall site by *Lin et al.* [2015]. They found ^{14}C ages for scarp-mantling talus of 2070 ± 30 and 2060 ± 30 years before present.

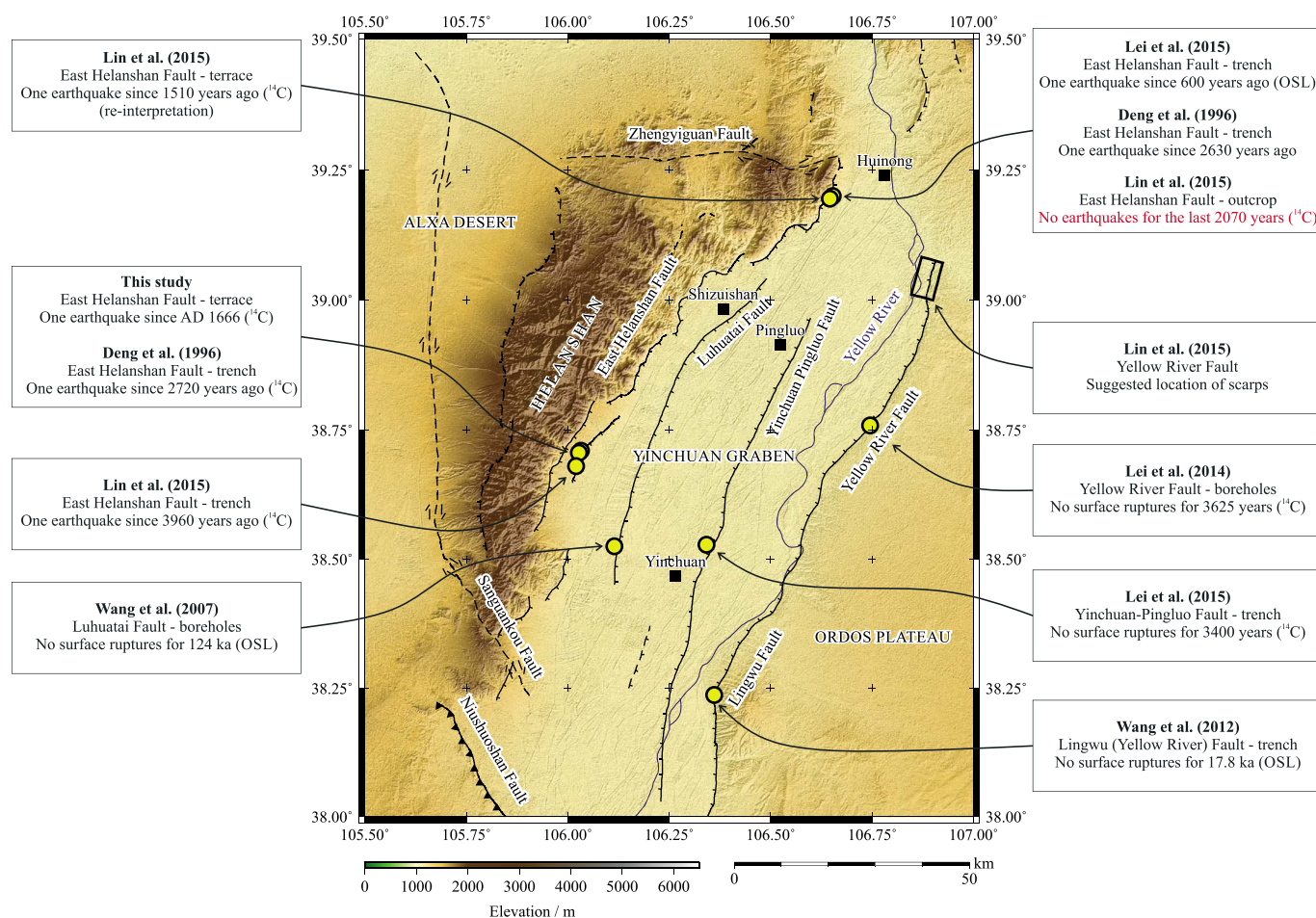


Figure 14. ASTER GDEM topography of the Yinchuan Graben. Faults, marked as thin black lines, have been mapped from satellite imagery (source: <http://earth.google.com>) based upon earlier fault maps from *Tapponnier and Molnar* [1977], *Zhang et al.* [1986] and *Deng and Liao* [1996]. Faults that are inferred or show no evidence of Quaternary activity are marked by dotted lines. Cities are marked by black squares. The Yellow River, which flows to the north, is marked in dark blue. Yellow circles mark sites where observations have been made about the recent activity of the four principal faults in the graben [Deng and Liao, 1996; Wang et al., 2007, 2012; Lei et al., 2014, 2015; Lin et al., 2015]. With the exception of one observation (in red) by Lin et al. [2015], all of the data are consistent with the East Helanshan Fault being the causative fault for the 1739 event.

However, on the basis of their outcrop photographs and sketches we were not able to verify the exact context of these samples. They also have ^{14}C ages of 1660 ± 30 and 1510 ± 30 years before present from a surface they label as T0, which they say is not offset. However, Google Earth imagery (for example, from 23rd February 2010) appears to show a fresh scarp in their T0 surface (at 38.680°N , 106.021°E), suggesting that the surface predates, rather than postdates, the most recent earthquake.

The combined evidence agrees with our conclusion and strongly suggests that the East Helanshan Fault was the primary causative structure, although we cannot completely rule out some additional subsurface slip on the Luhutai, Yinchuan-Pingluo and Yellow River Faults. As discussed in section 3, the fact that the greatest shaking was felt in the center of the graben is likely to be because the thick sediments [Zhang et al., 1990] amplified the seismic waves. Furthermore, if the seismic reflection data from Fang et al. [2009] is correct in saying that the Yellow River Fault was the major graben-forming structure (see Figure 2b), then this implies that the Yellow River Fault is no longer as active as it must have been in the past.

6.2. Characterizing the 1739 Earthquake

6.2.1. Throw Distribution

During our mapping of the East Helanshan scarps (see section 5.2) we were unable to resolve any lateral offsets either in the field or from the Pleiades DEM (except for the one site north of the Great Wall). We also made very few observations of fault dip. Nonetheless, at the road-cut site on the Suyukou scarps (see Figure 6c)

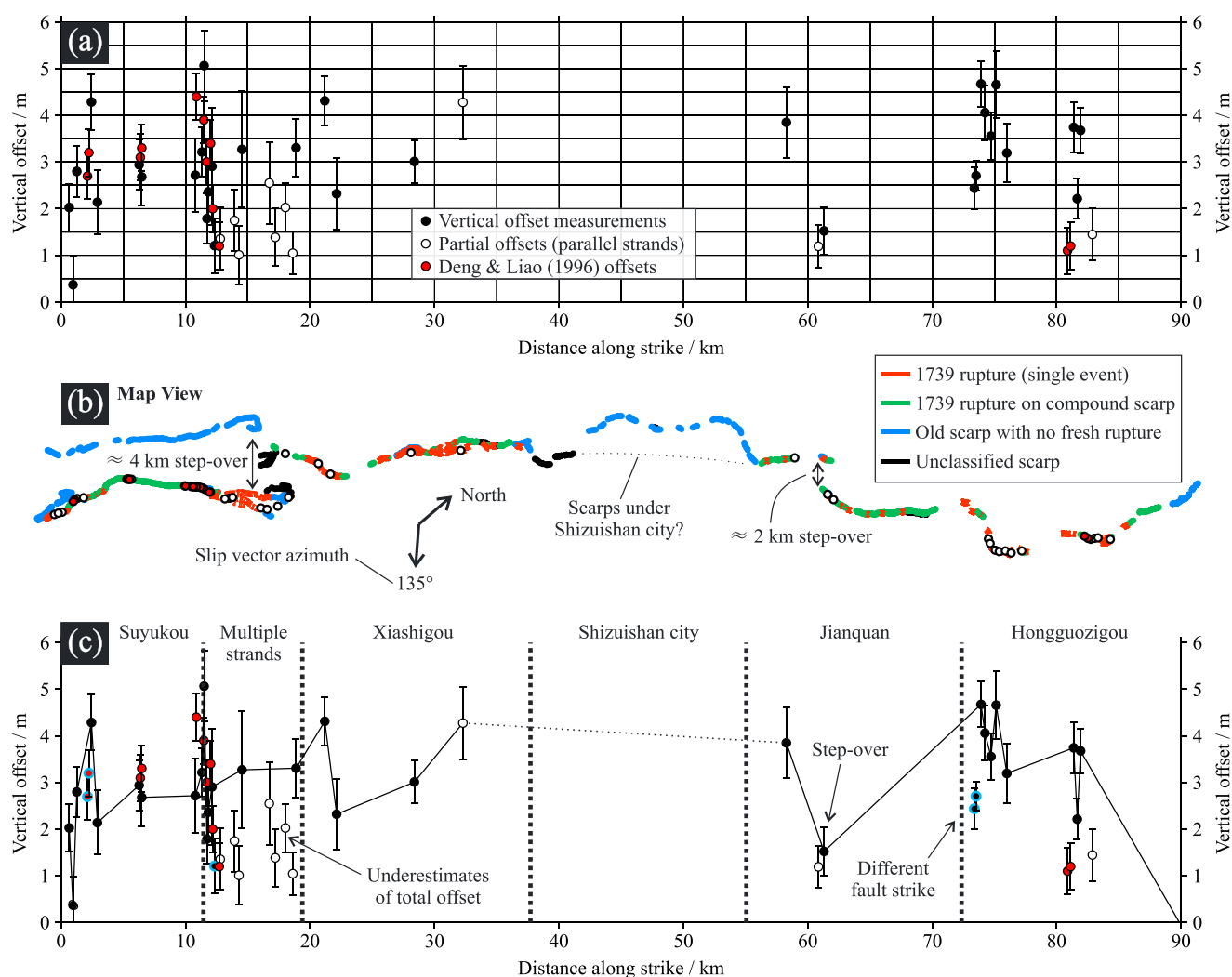


Figure 15. (a) Throw distribution (vertical offset versus distance along strike) for the 1739 Yinchuan earthquake. Points marked in white indicate locations where the measurement is unlikely to represent the total vertical offset because of the existence of parallel rupture strands. Red points are data from *Deng and Liao* [1996]. (b) Map view of fault scarps from the 1739 earthquake. Measurement points for data in this study are shown by white circles, and measurement points for data from *Deng and Liao* [1996] are shown by red circles. (c) Interpreted throw distribution containing the same data as in Figure 15a. Points ringed in blue indicate measurements made on sections with a significantly different local fault strike. The black line joins consecutive offset measurements along strike (from this study), excluding partial offsets and measurements with different local fault strike.

we measured a fault dip of 66° . The nearest throw measurement is 4.3 m, giving a slip of 4.7 m assuming pure dip-slip motion. Meanwhile, adjacent to the Great Wall on the central fault strand, *Liao and Pan* [1982] recorded a fault dip in their trench of 70° . Our nearest throw measurement from a location where there is only a single rupture strand is 3.9 m, giving a fault slip of 4.2 m. However, we do not have enough fault dip observations to be able to convert all of our vertical offset measurements into slip on the fault. We therefore plot the variation of throw along strike (see section 4 for a description of how these throw measurements were made). The position of each throw measurement was projected onto a straight line joining the two ends of the rupture in order to determine its distance along strike. The results are recorded in Table 2 and displayed in Figure 15a. *Deng and Liao* [1996] do not quote any errors on their results, so for this plot we have assumed errors of ± 0.5 m on their offset measurements.

The field data from *Deng and Liao* [1996] at the Suyukou scarps—for example, from 2 km, 6 km, and 11 km along strike—agrees well with our measurements, confirming that our DEM is of sufficiently high resolution to make such measurements. The two offsets from *Deng and Liao* [1996] on the Hongguozigou scarps of

1.1 and 1.2 m are, however, noticeably smaller than our results. During the measurement of our offsets we discarded the profiles from the locations immediately adjacent to the sites measured by *Deng and Liao* [1996] because the difference in slope above and below the scarp was more than 1° . Nonetheless, we obtained offsets of 2.1 and 3.0 m at roughly equivalent sites. It is possible that *Deng and Liao* [1996] did not adequately take account of the difference in slope angle when making their measurements.

Figure 15c is an attempt to estimate a throw distribution based on the point data shown in Figure 15a. Points ringed in blue indicate measurements where the local fault strike is significantly different to the overall average and therefore highlight places where we might expect to see a smaller vertical offset (see section 6.2.2). The black line joins consecutive offset measurements along strike (from this study), excluding partial offsets and measurements with a different local fault strike. The line returns to zero at a distance of nearly 90 km, corresponding to our field site at 39.262°N , 106.671°E where no sign of recent rupture was observed. As expected, most of the partial offset measurements fall below this line, for example, along the section between 12 and 19 km along strike. At a distance of approximately 12 km, toward the northern end of the Suyukou scarps, there is a throw minimum as the fault splits into multiple strands and approaches the step over. Similarly, at a distance of about 61 km, at the step over within the Jianquan segment, there is a second throw minimum. These throw minima at fault step overs may imply that the segments either side do not yet form a continuous, through-going structure at depth [*Kim and Sanderson*, 2005].

In section 5.2.2 we noted that no surface fault scarps were seen along the central section of the rupture, behind Shizuishan city. The range front is embayed at this location (see Figure 15b), so one possible explanation for the lack of scarps is that the 1739 rupture cut off this corner in the range front and went through what is now the center of the city. Rapid urban sprawl could have since removed all traces of this portion of the rupture. Another possibility is that there were no original surface ruptures on this section of the fault. This would further imply that the 1739 earthquake occurred as two separate subevents, an idea that would be consistent with the historical records that mention ground shaking continuing for two whole hours [*Zhang et al.*, 1986]. We do not have sufficient data to definitively adjudicate between these two hypotheses. However, we note that the measured throws at sites either side of Shizuishan city (see Figure 15c) do not appear to be tailing off in the way that we might expect for the ends of fault segments (according to an elliptical growth model), indicating that two subevents is perhaps less likely [*Peacock*, 2002; *Kim and Sanderson*, 2005].

6.2.2. Slip Vector Azimuth

We were not able to observe any fault plane exposures and so could not measure the orientations of any striations. However, there are two other ways in which we can estimate the slip vector azimuth. First, although we have no way of verifying the previous measurements from the Great Wall site, we can try using them to see what they suggest about the slip direction (see section 5.2.4). *Zhang et al.* [1986] recorded a cumulative vertical offset across the three fault strands at this site of 2.7 m. Combined with an average fault dip of 72° from the three trenches opened adjacent to the Great Wall by *Liao and Pan* [1982], we obtain fault-normal motion of 0.9 m. *Zhang et al.* [1986] also recorded cumulative right-lateral motion of 3 m, enabling us to estimate that the slip vector is 164° from the strike direction. The average local fault strike measured by *Liao and Pan* [1982] is 30° , giving us a slip vector azimuth of 194° .

The second method makes use of the observation, noted in section 5.2, that there are a few locations where the rupture changes strike by 70° over a length scale of less than 100 m (see Figure 16b). At rupture bends such as this one we observe a marked change in the throw on moving round the bend, and we can use this change to estimate the slip vector azimuth. Predicting how throw is expected to vary with local fault strike would require detailed knowledge of the fault dip and assumptions about how the orientation of the slip vector might change along strike. However, we note that for uniform horizontal extension along the whole fault length, the fault-perpendicular motion (and hence the vertical offset due to this component of the slip) will be greatest for portions of the fault that are perpendicular to the slip vector azimuth.

Figure 16a shows our vertical offset measurements plotted against local fault strike. The black curve approximately envelopes that data and is intended only to illustrate that there is a broad peak in the data at around 40 to 50° , suggesting a slip vector azimuth perpendicular to this orientation (i.e., 130 to 140°). This result is consistent with the example shown in Figure 16b. Here the clearest scarps are those striking at around 40 to 50° . This is also borne out by the topographic profiles in Figures 16c–16f. Profiles A–A' and B–B' are from segments with strikes of 91° and 101° and show vertical offsets of 2.4 and 2.7 m, respectively. Meanwhile, profiles C–C' and D–D' are from segments with strikes of 35° and 31° and show vertical offsets of 4.7 and 4.1 m.

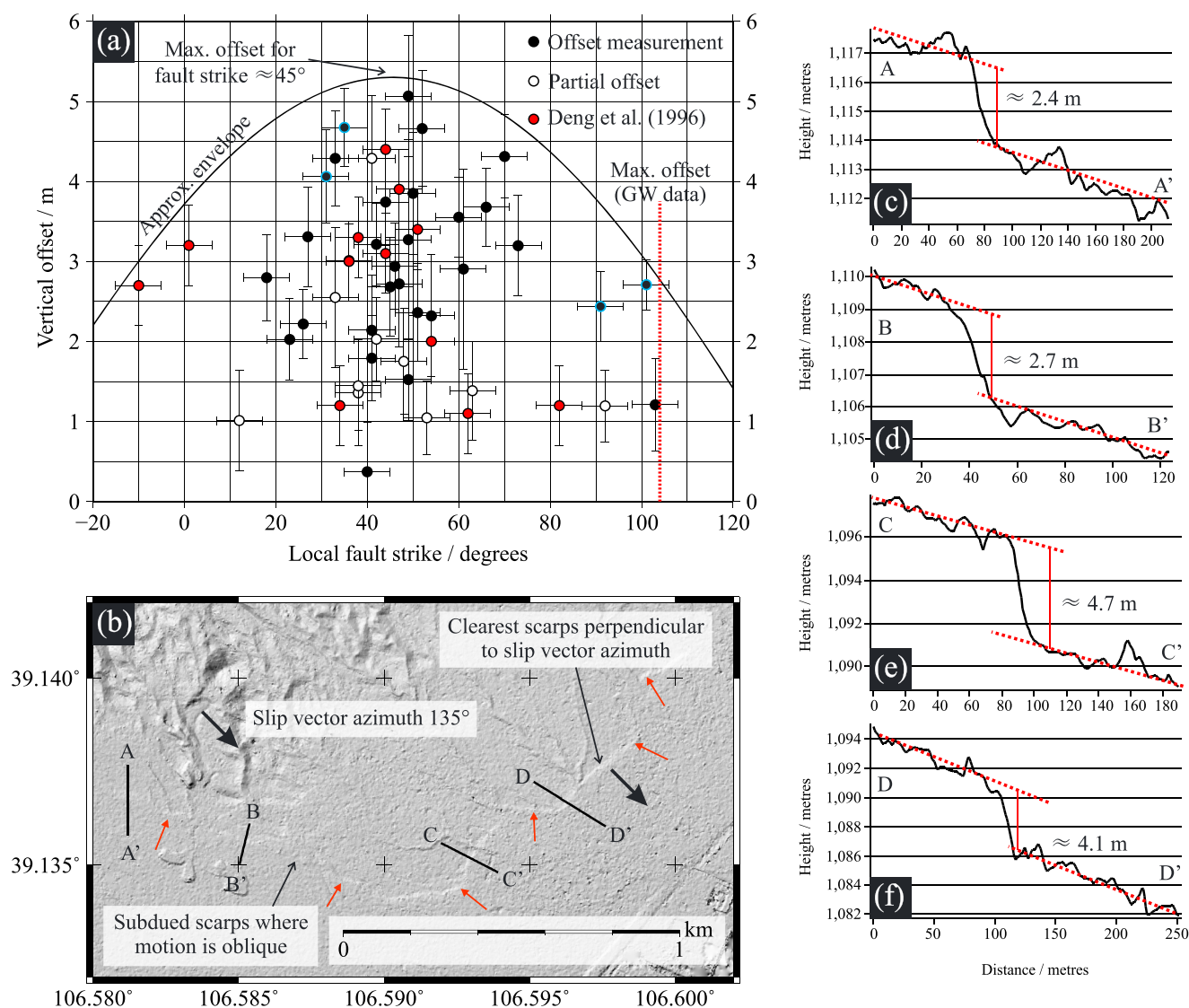


Figure 16. (a) Plot of vertical offset measured on the Pleiades DEM against local fault strike. Points marked in white indicate locations where the measurement is unlikely to represent the total vertical offset because of the existence of parallel rupture strands. Red points are data from *Deng and Liao* [1996]. Points ringed in blue are measurements from the sites shown in Figure 16b. The black curve is an approximate data envelope. The dotted red line indicates the local fault strike (104°) for which we would expect the maximum vertical offset based on the slip vector azimuth calculated from the data at the Great Wall site. (b) Zoomed in view of the DEM at a location on the Hongguozigou segment where the fault (marked by red arrows) changes strike abruptly by about 70° . The largest scarps (illuminated in white) occur along segments striking at approximately 45° , perpendicular to the suggested slip vector azimuth of 135° . (c–f) Topographic profiles at the locations marked in Figure 16b to show the difference in scarp height when the local fault strike is different. Note the varying scales on these plots.

However, there remains a large discrepancy between the slip vector azimuth of 194° from the Great Wall measurements and the slip vector azimuth of 130 to 140° from our data. The dotted red line on Figure 16a indicates the fault strike at which we would expect the largest vertical offset (104°) if the Great Wall measurements are correct, and it is noticeably displaced from the observed peak. If this discrepancy is real it could indicate either a significant change in slip vector azimuth at the northernmost end of the rupture or a spatial partitioning of dip-slip and strike-slip motion. For example, almost pure normal motion on the East Helanshan Fault could be accompanied by right-lateral motion on a fault or faults within the graben for the majority of its length south of the Great Wall. Our single field site north of the Great Wall (see Figures 13c and 13d) did appear to show evidence of right-lateral offsets (see section 5.2.4), but rotation of the slip vector, the presence of partitioned faulting, and whether or not the 1739 earthquake involved additional slip on parallel structures, all remain speculative.

Table 3. Fault Parameters and Magnitude Estimates

Parameter	Best Estimate	Upper Bound
<i>Fault Parameters</i>		
Fault length (km)	87	94
Seismogenic thickness (km)	20	28 ^a
Fault dip (deg)	39	39 ^a
Surface fault dip (deg)	66	66
Down-dip width (km)	32	44
Fault area (km ²)	2765	4182
Maximum throw (m)	5.1	8.0
Maximum slip (m)	5.6	8.8
Average throw (m)	3.0	4.5
Average slip (m)	3.3	4.9
Slip-length ratio (β)	3.8×10^{-5}	5.2×10^{-5}
<i>Magnitude Estimates</i>		
M_w from fault length ^b	7.4	7.5
M_w from fault plane area ^b	7.4	7.6
M_w from maximum slip ^b	7.2	7.3
M_w from average slip ^b	7.1	7.2
M_w from $M_0 = \mu A \bar{u}$	7.6	7.8

^a28 km seismogenic thickness and 39° fault dip from Fang *et al.* [2009].

^bScaling relationships from Wells and Coppersmith [1994].

6.2.3. Estimating the Magnitude

In this section we estimate a range of possible magnitudes for the 1739 earthquake based on observations and measurements made in this study. However, we also consider the likely upper bounds on all the relevant parameters in order to work out the maximum conceivable magnitude for the event (see Table 3).

According to our mapping, the end-to-end length of the 1739 rupture is 87 km (see section 5.2 and Figure 3). However, it is not clear to what extent the surface salients and embayments reflect the deeper fault structure. If we assume that some of the surface sinuosity does reflect real changes at depth and use a rupture trace made of 10 points, with 1 point approximately every 10 km, we obtain a rupture length of 94 km. We therefore take 94 km as our upper bound on fault length.

The maximum throw measured in this study is 5.1 m (see Table 2). Assuming the surface fault dip of 66° measured at the road-cut exposure is representative (see Figure 6) and that motion is pure dip slip, the maximum slip on the fault plane at the surface is 5.6 m. Similarly, the average throw measured in this study is 3.0 m, and again, assuming a fault dip of 66°, we obtain an average slip of 3.3 m.

However, we are missing data for the central portion of the rupture, between 32 and 58 km along strike (see Figure 15), and assuming that there were not two separate subevents, it is in the central portion that we might expect the maximum throw [e.g., Peacock, 2002; Kim and Sanderson, 2005 and Faure Walker *et al.*, 2009]. We therefore propose taking upper bounds on the maximum and average throw of 8 m and 4.5 m, respectively, giving upper bounds on the maximum and average slip (using a dip of 66°) of 8.8 m and 4.9 m, respectively.

We estimate down-dip width from seismogenic thickness and fault dip at depth. Cheng *et al.* [2014] note that most earthquakes in the vicinity of the Yinchuan Graben occur above 20 km. This is in agreement with previous estimates of seismogenic thickness by Wesnousky *et al.* [1984] and Molnar and Deng [1984]. Estimates of the subsurface fault dip based on seismic reflection data vary from 39° [Fang *et al.*, 2009] to approximately 60° [He *et al.*, 2005; Liu *et al.*, 2008]. Here, though, we use the dip of 39° from Fang *et al.* [2009] since it is the only available seismic reflection profile that goes deep enough to include the whole seismogenic layer. (We also note that the maximum down-dip width is obtained for the shallowest fault dip at depth.) In combination with the seismogenic thickness of 20 km, we obtain a down-dip width of 32 km and a fault plane area of 2765 km². However, Fang *et al.* [2009] also suggest from their seismic reflection data that the base of the East Helanshan

Fault can be traced to a depth of 28 km. If this is correct and the whole fault is seismogenic, we find upper bounds of 44 km for down-dip width and 4182 km² for fault plane area.

Applying scaling relationships between moment magnitude and each of fault length, fault plane area, maximum slip, and average slip, we obtain M_w 7.4, M_w 7.4, M_w 7.2, and M_w 7.1, respectively [Wells and Coppersmith, 1994]. Using the same relationships with our upper bounds gives M_w 7.5, M_w 7.6, M_w 7.3, and M_w 7.2, respectively. We also calculate seismic moment (M_0) using the relationship $M_0 = \mu A \bar{u}$. Using a modulus of rigidity of 3×10^{10} Pa and the parameters listed above, we obtain a best estimate seismic moment of 2.72×10^{20} Nm and an upper bound of 6.18×10^{20} Nm, which correspond to moment magnitudes of 7.6 and 7.8. Finally, we also calculate slip-to-length ratios of 3.8×10^{-5} and 5.2×10^{-5} for our best estimate and upper bound parameters, respectively. Table 3 lists all of these results and the parameters required to make the estimates.

Our data suggests that the previously proposed magnitude of 8.0 [Zhang et al., 1986; State Seismological Bureau and Fudan University, 1990] may be an overestimate of the size of the 1739 earthquake due to amplification effects within the graben sediments. On the basis of the various fault parameters obtained in this study we suggest a preferred magnitude in the range M_w 7.1 to M_w 7.6. A M_w 7.8 event is only found by taking the upper bound for every single parameter. Even if motion also occurred at depth on faults within the graben interior, a M_w 8.0 event would require an additional moment release of 5.5×10^{20} Nm, equivalent to slip of approximately 10 m on one of these other faults (using $M_0 = \mu A \bar{u}$ and our upper bound of M_w 7.8 for the motion on the East Helanshan Fault).

Our results therefore put the Yinchuan earthquake in line with other earthquakes that have been observed in the instrumental period such as the $M7.6$ Pleasant Valley and $M7.3$ Hebgen Lake events, though these earthquakes had shorter rupture lengths (of 60 and 30 km, respectively) [Jackson and White, 1989]. Similarly, our best estimate slip-to-length ratio of 3.8×10^{-5} is in accord with generally accepted values of between 10^{-5} to 10^{-4} [Scholz, 1982, 2002]. In other words, the 1739 Yinchuan earthquake, though still a major normal-faulting event, is not extraordinarily large and unique circumstances do not need to be invoked in order to understand its occurrence.

In terms of future seismic hazard, the reduced magnitude estimate indicates that a smaller earthquake than previously thought caused the intensity of shaking and amount of damage that was observed in 1739. In addition, the reduced magnitude estimate implies an increased frequency of such earthquakes; a recurrence interval that is 57% shorter (assuming a slip-to-length ratio of 5×10^{-5}) is needed to accommodate a given strain rate across the East Helanshan Fault with M_w 7.6 events rather than M_w 8.0 events.

7. Conclusions

¹⁴C dating very strongly suggests that the Suyukou scarps, at the southern end of the East Helanshan rupture, are from 1739. The similar morphology of other scarps along the same range front, with a characteristic free face, also strongly suggests that the East Helanshan Fault was the causative fault for the 1739 event. Our Pleiades DEM (with an horizontal resolution of 1 to 2 m) was shown to be of sufficiently high quality to enable much of the 1739 rupture to be mapped, thereby significantly extending what is known from field observations alone. Recent landscape modification at the controversial Great Wall site has made previous studies hard to assess, but observations of the scarps either side confirm that the wall must have been offset in 1739. Measurements of vertical displacement and local fault strike indicate a slip vector azimuth of 130 to 140° in the 1739 earthquake. We also measure a total rupture length of 87 km, a maximum throw of 5.1 m and an average throw of 3.0 m. Based on our best estimate fault parameters we calculate a moment magnitude for the earthquake in the range M_w 7.1 to M_w 7.6.

This study of the 1739 earthquake in the Yinchuan Graben has demonstrated the importance of using geological data preserved in the landscape and up-to-date surveying techniques to reexamine historical earthquakes. We have also shown how high-resolution satellite-derived DEMs can be employed in tectonic studies to make detailed measurements of individual earthquake ruptures. Furthermore, given the rapid urban expansion and extensive human modification of the landscape in our study region, our data provides an important archive of the geomorphological evidence associated with this earthquake. Together, the geological data and new techniques have enabled us to provide further, tight constraints on the principal causative fault for the 1739 event and to discover that the earthquake was not as large, or as extraordinary, as previously thought.

Acknowledgments

The Pleiades DEM can be downloaded from OpenTopography (<http://www.opentopography.org/>) and a KML file of our rupture map is available on request. Most of the figures in this paper were made using GMT [Wessel et al., 2013]. ASTER GDEM is a product of METI and NASA. This research has been supported by the Natural Environment Research Council (NERC) through a studentship awarded to TAM, the Centre for Observation and Modelling of Earthquakes, Volcanoes and Tectonics (COMET), the Looking inside the Continents from Space (LICS) large grant, and the NERC/ESRC Earthquakes without Frontiers (EwF) consortium. We are grateful to Peizhen Zhang and our colleagues at the China Earthquake Administration (CEA) for their assistance with fieldwork; Owen Green, Stephen Harris, Richard Staff, and the Oxford Radiocarbon Accelerator Unit (ORAU) for their help identifying and preparing our ^{14}C samples for dating; Al Sloan, John Elliott, and David Mackenzie for helpful discussions; and Steve Angster for an introduction to the 1954 Dixie Valley rupture in the field. We also wish to thank Alex Whittaker and an anonymous reviewer for their helpful comments on the manuscript.

References

- Bai, M., and D. Jiao (2005), The historical analysis for $M = 8$ earthquake in 1739 at Yinchuan-Pingluo area [in Chinese], *Northwestern Seismol. J.*, 27(2), 135–140.
- Bilham, R., and P. England (2001), Plateau ‘pop-up’ in the great 1897 Assam earthquake, *Nature*, 410(6830), 806–809, doi:10.1038/35071057.
- Brock, F., T. Higham, P. Ditchfield, and C. Bronk (2010), Current pretreatment methods for AMS radiocarbon dating at the Oxford Radiocarbon Accelerator Unit (ORAU), *Radiocarbon*, 52(1), 103–112.
- Bronk, C., R. Thomas, and H. Philip (2004), Towards high-precision AMS: Progress and limitations, *Radiocarbon*, 46(1), 17–24.
- Bronk Ramsey, C., and S. Lee (2013), Recent and planned developments of the Program OxCal, *Radiocarbon*, 55(2–3), 720–730, doi:10.2458/azu_js_rc.55.16215.
- Caskey, S. J., S. G. Wesnousky, P. Zhang, and D. B. Slemmons (1996), Surface Faulting of the 1954 Fairview Peak (M_s 7.2) and Dixie Valley (M_s 6.8) Earthquakes [in Chinese], Central Nevada, *Bull. Seismol. Soc. Am.*, 86(3), 761–787.
- Chai, C., et al. (2006), Comprehensive multi-level exploration of buried active fault: An example of Yinchuan buried active fault [in Chinese], *Seismolog. Geol.*, 28(4), 536–546.
- Cheng, B., S. Cheng, G. Zhang, and D. Zhao (2014), Seismic structure of the Helan-Liupan-Ordos western margin tectonic belt in North-Central China and its geodynamic implications, *J. Asian Earth Sci.*, 87, 141–156, doi:10.1016/j.jseas.2014.01.006.
- Copley, A., J.-P. Avouac, J. Hollingsworth, and S. Leprince (2011), The 2001 M_w 7.6 Bhuj earthquake, low fault friction, and the crustal support of plate driving forces in India, *J. Geophys. Res.*, 116, B08405, doi:10.1029/2010JB008137.
- Copley, A., J. Hollingsworth, and E. Bergman (2012), Constraints on fault and lithosphere rheology from the coseismic slip and postseismic afterslip of the 2006 M_w 7.0 Mozambique earthquake, *J. Geophys. Res.*, 117, B03404, doi:10.1029/2011JB008580.
- Darby, B. J., and B. D. Ritts (2002), Mesozoic contractional deformation in the middle of the Asian tectonic collage: The intraplate Western Ordos fold-thrust belt, China, *Earth Planet. Sci. Lett.*, 205(1–2), 13–24, doi:10.1016/S0012-821X(02)01026-9.
- Deng, Q., and Y. Liao (1996), Paleoseismology along the range-front fault of Helan Mountains, north central China, *J. Geophys. Res.*, 101, 5873–5893.
- Deng, Q., Y. Wang, Y. Liao, W. Zhang, and M. Li (1984), Colluvial wedges and Holocene activity along the range-front fault of Helan Shan [in Chinese], *Chin. Sci. Bull.*, 29, 557–560.
- Ding, M. (1981), Some paleoseismic evidence in the north China region [in Chinese], *Seismolog. Geol.*, 3(1), 67–74.
- Ekström, G., M. Nettles, and A. Dziewonski (2012), The global CMT project 2004–2010: Centroid-moment tensors for 13,017 earthquakes, *Phys. Earth Planet. Inter.*, 200–201, 1–9, doi:10.1016/j.pepi.2012.04.002.
- Fang, S., C. Zhao, C. Chai, B. Liu, S. Feng, M. Liu, Q. Lei, and H. Liu (2009), Seismological evidences of the crustal structures and tectonics in the Yinchuan Downfaulted Basin, *Chin. J. Geophys.*, 52(5), 1101–1110, doi:10.1002/cjg2.1435.
- Farr, T. G., and M. Kobrick (2000), Shuttle radar topography mission produces a wealth of data, *Eos Trans. AGU*, 81(48), 583–585.
- Faure Walker, J. P., G. P. Roberts, P. A. Cowie, I. D. Papanikolaou, P. R. Sammonds, A. M. Michetti, and R. J. Phillips (2009), Horizontal strain-rates and throw-rates across breached relay zones, central Italy: Implications for the preservation of throw deficits at points of normal fault linkage, *J. Struct. Geol.*, 31(10), 1145–1160, doi:10.1016/j.jsg.2009.06.011.
- Hanks, T. C., and H. Kanamori (1979), A moment magnitude scale, *J. Geophys. Res.*, 84(B5), 2348–2350, doi:10.1029/JB084iB05p02348.
- He, J., Y. Li, and C. Teng (2005), Asymmetric flank uplift of the Yinchuan graben, north central China: Implications for lateral variation of crustal rheology from the Alashan to the Ordos, *Geophys. Res. Lett.*, 32, L23302, doi:10.1029/2005GL023661.
- International Seismological Centre (2013), *On-Line Bulletin*, Int. Seismic Cent., Thatcham, U. K.
- Jackson, J., and M. Leeder (1994), Drainage systems and the development of normal faults: An example from Pleasant Valley, Nevada, *J. Struct. Geol.*, 16(8), 1041–1059.
- Jackson, J. A., and N. J. White (1989), Normal faulting in the upper continental crust: Observations from regions of active extension, *J. Struct. Geol.*, 11(1–2), 15–36.
- Kim, Y. S., and D. J. Sanderson (2005), The relationship between displacement and length of faults: A review, *Earth Sci. Rev.*, 68(3–4), 317–334, doi:10.1016/j.earscirev.2004.06.003.
- Lee, W. H. K., F. T. Wu, and C. Jacobsen (1976), A catalog of historical earthquakes in China compiled from recent Chinese publications, *Bull. Seismol. Soc. Am.*, 66(6), 2003–2016.
- Lee, W. H. K., F. T. Wu, and S. C. Wang (1978), A catalog of instrumentally determined earthquakes in China (magnitude greater than 6) compiled from various sources, *Bull. Seismol. Soc. Am.*, 68(2), 383–398.
- Lei, Q., C. Chai, G. Meng, P. Du, Y. Wang, X. Xie, and X. Zhang (2008), Composite drilling section exploration of Yinchuan Buried Fault [in Chinese], *Seismol. Geol.*, 30(1), 250–263.
- Lei, Q., C. Chai, W. Zheng, P. Du, X. Xie, Y. Wang, J. Cui, and G. Meng (2014), Activity and slip rate of the northern section of Yellow River Fault revealed by drilling [in Chinese], *Seismol. Geol.*, 36(2), 464–477.
- Lei, Q., C. Chai, P. Du, J. Yu, X. Xie, and Y. Wang (2015), Re-discussion of the seismogenic structure of the $M8.0$ Pingluo earthquake in 1739 [in Chinese], *Seismol. Geol.*, 37(2), 413–429.
- Li, M., and Z. Wan (1984), Characteristics of the earthquake-generating structures for magnitude 8.0 Pingluo earthquake of 1739 and the process of its preparation [in Chinese], *Seismol. Geol.*, 6(3), 23–28.
- Li, Y., G. Yang, Z. Li, L. Guo, C. Huang, W. Zhu, Y. Fu, Q. Wang, Z. Jiang, and M. Wang (2003), Movement and strain conditions of active blocks in the Chinese mainland, *Sci. China, Ser. D Earth Sci.*, 46, 82–117, doi:10.1360/Dz0008.
- Liao, Y., and Z. Pan (1982), Dislocation of the great wall in the Hongguozigou, Ningxia autonomous region [in Chinese], *Seismol. Geol.*, 4(2), 77–80.
- Lin, A., G. Rao, J. Hu, and W. Gong (2013), Reevaluation of the offset of the Great Wall associated with the ca. $M8.0$ Pingluo earthquake of 1739, Yinchuan graben, China, *J. Seismolog.*, 17(4), 1281–1294, doi:10.1007/s10950-013-9391-2.
- Lin, A., J. Hu, and W. Gong (2015), Active normal faulting and the seismogenic fault of the 1739 $M8.0$ Pingluo earthquake in the intracontinental Yinchuan Graben, China, *J. Asian Earth Sci.*, 114, 155–173, doi:10.1016/j.jseas.2015.04.036.
- Liu, B. J., C. Z. Chai, S. Y. Feng, C. B. Zhao, and H. K. Yuan (2008), Seismic exploration method for buried fault and its up-breakpoint in Quaternary sediment area - An example of Yinchuan buried active fault, *Chin. J. Geophys.*, 51(5), 1475–1483.
- Liu, G. (2000), The Cenozoic rift system of the North China Plain and the deep internal process, *Tectonophysics*, 133(1987), 277–285.
- Liu, J., P. Zhang, D. Zheng, J. Wan, W. Wang, P. Du, and Q. Lei (2010), Pattern and timing of late Cenozoic rapid exhumation and uplift of the Helan Mountain, China, *Sci. China Earth Sci.*, 53(3), 345–355, doi:10.1007/s11430-010-0016-0.
- Liu, M., S. Stein, and H. Wang (2011), 2000 years of migrating earthquakes in North China: How earthquakes in midcontinents differ from those at plate boundaries, *Lithosphere*, 3(2), 128–132, doi:10.1130/L129.1.
- Molnar, P., and Q. Deng (1984), Faulting associated with large earthquakes and the average rate of deformation in central and eastern Asia, *J. Geophys. Res.*, 89, 6203–6227.

- Parsons, B., Y. Zhou, J. R. Elliott, I. Barisin, and R. T. Walker (2014), Assessing the ability of pleiades stereo imagery to determine height changes in earthquakes: A case study for the El Mayor-Cucapah Epicentral area. Abstracts EP43E-08 presented at 2014 Fall Meeting, AGU, San Francisco, Calif., 15–19 Dec.
- Peacock, D. (2002), Propagation, interaction and linkage in normal fault systems, *Earth Sci. Rev.*, 58(1–2), 121–142, doi:10.1016/S0012-8252(01)00085-X.
- Reimer, P., et al. (2013), IntCal13 and Marine13 radiocarbon age calibration curves 0–50,000 years cal BP, *Radiocarbon*, 55(4), 1869–1887, doi:10.2458/azu_js_rc.55.16947.
- Scholz, C. H. (1982), Scaling laws for large earthquakes: Consequences for physical models, *Bull. Seismol. Soc. Am.*, 72(1), 1–14.
- Scholz, C. H. (2002), *The Mechanics of Earthquakes and Faulting*, 2nd ed., 504 pp., Cambridge Univ. Press, Cambridge, U. K.
- State Seismological Bureau, I. o. G., and I. o. C. H. G. Fudan University (1990), *Atlas of the Historical Earthquakes in China (the Qing Dynasty period)* [in Chinese], 244 pp., China Cartographic House, Beijing.
- Tapponnier, P., and P. Molnar (1977), Active faulting and tectonics in China, *J. Geophys. Res.*, 82(20), 2905–2930.
- Wang, Q., et al. (2001), Present-day crustal deformation in China constrained by global positioning system measurements, *Science*, 294, 574–577, doi:10.1126/science.1063647.
- Wang, X., C. Chai, P. Du, Q. Lei, G. Yin, and Y. Lu (2012), Luminescence age constraints on palaeo-earthquake events along the Lingwu fault in the Yinchuan Basin, China, *Geochronometria*, 39(1), 57–61, doi:10.2478/s13386-011-0051-4.
- Wang, Y., P. Du, and Q. Lei (2007), Summary on recent progress of active fault exploration project in Yinchuan City [in Chinese], *Technol. Earthquake Disaster Prev.*, 2(2), 166–175.
- Wells, D. L., and K. J. Coppersmith (1994), New empirical relationships among magnitude, rupture length, rupture width, rupture area, and surface displacement, *Bull. Seismol. Soc. Am.*, 84(4), 974–1002.
- Wesnousky, S. G., L. M. Jones, C. H. Scholz, and Q. Deng (1984), Historical seismicity and rates of crustal deformation along the margins of the Ordos block, North China, *Bull. Seismol. Soc. Am.*, 74(5), 1767–1783.
- Wessel, P., W. H. F. Smith, R. Scharroo, J. Luis, and F. Wobbe (2013), Generic mapping tools: Improved version released, *Eos Trans. AGU*, 94(45), 409–410, doi:10.1002/2013EO450001.
- Zhang, B., Y. Liao, S. Guo, R. E. Wallace, R. C. Bucknam, and T. C. Hanks (1986), Fault scarps related to the 1739 earthquake and seismicity of the Yinchuan Graben, Ningxia Huizu Zizhiqu, China, *Bull. Seismol. Soc. Am.*, 76(5), 1253–1287.
- Zhang, P., B. C. Burchfiel, P. Molnar, W. Zhang, D. Jiao, Q. Deng, Y. Wang, L. Royden, and F. Song (1990), Late Cenozoic tectonic evolution of the Ningxia-Hui Autonomous Region, China, *Geol. Soc. Am. Bull.*, 102(11), 1484–1498, doi:10.1130/0016-7606(1990)102<C1484:LCTEOT>2.3.CO;2.
- Zhang, W., Y. Liao, and Z. Pan (1982), On the piedmont scarp in diluvial fan of Mt. Helanshan [in Chinese], *Seismolog. Geol.*, 4(2), 32–34.
- Zhang, Y., J. L. Mercier, and P. Vergely (1998), Extension in the graben systems around the Ordos (China), and its contribution to the extrusion tectonics of south China with respect to Gobi-Mongolia, *Tectonophysics*, 285, 41–75.
- Zhao, B., X. Xie, C. Chai, H. Ma, X. Xu, D. Peng, W. Yin, and J. Tao (2007a), Imaging the graben structure in the deep basin with a microtremor profile crossing the Yinchuan City, *J. Geophys. Eng.*, 4(3), 293–300, doi:10.1088/1742-2132/4/3/S08.
- Zhao, H., C. Liu, F. Wang, J. Wang, Q. Li, and Y. Yao (2007b), Uplift and evolution of Helan Mountain, *Sci. China, Ser. D Earth Sci.*, 50(S2), 217–226, doi:10.1007/s11430-007-6010-5.
- Zhou, Y., J. R. Elliott, B. Parsons, and R. T. Walker (2015), The 2013 Balochistan earthquake: An extraordinary or completely ordinary event?, *Geophys. Res. Lett.*, 42, 6236–6243, doi:10.1002/2015GL065096.